

Geometric Integrator for Langevin Systems with Quaternion-based Rotational Degrees of Freedom and Hydrodynamic Interactions

R. L. Davidchack,^{1, a)} T. E. Ouldridge,^{2, b)} and M. V. Tretyakov^{3, c)}

¹⁾*Department of Mathematics, University of Leicester, Leicester, LE1 7RH, UK*

²⁾*Department of Bioengineering, Imperial College London, London SW7 2AZ, UK*

³⁾*School of Mathematical Sciences, University of Nottingham, Nottingham, NG7 2RD, UK*

We introduce new Langevin-type equations describing the rotational and translational motion of rigid bodies interacting through conservative and non-conservative forces, and hydrodynamic coupling. In the absence of non-conservative forces the Langevin-type equations sample from the canonical ensemble. The rotational degrees of freedom are described using quaternions, the lengths of which are exactly preserved by the stochastic dynamics. For the proposed Langevin-type equations, we construct a weak 2nd order geometric integrator which preserves the main geometric features of the continuous dynamics. A number of numerical experiments are presented to illustrate both the new Langevin model and the numerical method for it.

Keywords. rigid body dynamics; quaternions; hydrodynamic interactions; Stokesian dynamics; canonical ensemble; Langevin equations; stochastic differential equations; weak approximation; ergodic limits; stochastic geometric integrators.

AMS 2000 subject classification. 82C31, 65C30, 60H10, 60H35.

I. INTRODUCTION

When modelling colloidal suspensions or solvated macromolecules, it is often convenient to treat the solvent molecules implicitly, thereby reducing the computational requirements of simulation^{1,2}. When doing so, an effective potential energy (in reality a free energy) is constructed between the remaining solute degrees of freedom². This effective potential, incorporating both direct and solvent-mediated contributions to the system's energy, can in principle reproduce the equilibrium distribution of the solute molecules having marginalised over the solvent configuration.

A given effective potential specifies the system's equilibrium distribution, but not its dynamics. Multiple dynamical models will in fact reach the same equilibrium distribution (see e.g. Refs. 2–4 and references therein). If dynamical properties are of interest, therefore, it is necessary to consider which of the possible dynamical models is most reasonable. One approach – Langevin dynamics – is to calculate generalised forces from the effective potential, and augment the resultant differential equations for the solute motion with additional noise and drag forces^{1,5}. These added forces model collisions with the implicit solvent and lead to diffusive motion of the solute particles.

A common approximation is to assume that the random and drag forces acting on each solute particle are independent. However, it is well-known that moving through a fluid sets up long-range flow fields that influence the drag experienced by other solute particles¹.

These hydrodynamic interactions (HI) are often of fundamental importance to system properties. Famously, the presence of HI alters the scaling of polymer diffusion coefficients with length⁶. HI are known to strongly influence the rheological⁷ and sedimentation⁸ properties of colloid suspensions, and are necessary to account for the diffusive behaviour of proteins within the cell^{9,10}. Hydrodynamic coupling is also central to the motion and interaction of microscopic swimmers^{11,12}.

In the low Reynolds number limit, the hydrodynamic force experienced by a single solute particle is linear in the velocities of all particles¹. Hydrodynamic interactions in the Langevin formalism can then be encoded through a *friction matrix*¹, which relates the force experienced to the particle velocities. The friction matrix, and its inverse the mobility matrix, are in general dense and depend on the configuration of the system in a complex manner. Many approximations exist for calculating these matrices given a configuration (extensively reviewed in Ref. 1), including methods for both long-range behaviour and so-called “lubrication theory” which applies at short distances.

Given the functional form of the friction/mobility matrix, along with the effective potential, stochastic integrators can be constructed to implement the resultant “Stokesian” dynamics. Ermak and McCammon's original first-order Euler-type integrator¹³ is still widely used^{7,9,10}. This scheme assumes an overdamped limit, eliminating the particle momenta and directly updating particle positions based on the forces and mobility matrix. The method was subsequently generalised to incorporate rotational motion of solute particles^{14,15}. However, implementing rotational motion using, for example, Euler angles, can be problematic due to singularities in the equations of motion¹⁶.

Unit quaternions, 4-dimensional unit vectors that can

^{a)}Electronic mail: r.davidchack@le.ac.uk

^{b)}Electronic mail: t.ouldridge@imperial.ac.uk

^{c)}Electronic mail: Michael.Tretyakov@nottingham.ac.uk

represent rigid-body orientation in 3D, are an alternative to Euler angles that avoid these singularities¹⁶. Recently, several quaternion-based integrators have been demonstrated for Langevin dynamics in the absence of HI, both in the overdamped limit^{17–19} and beyond^{17,19}. To date, however, little has been done to incorporate HI into quaternion-based integrators (a scheme is proposed in Ref. 18, but not tested).

In this article we derive quaternion-based Langevin equations for the Stokesian dynamics of rigid bodies, based on the Hamiltonian description of rigid-body dynamics in Ref. 20 and its extension to Langevin dynamics without HI in Refs. 17 and 19. We then derive and demonstrate performance of a weak second-order geometric integrator building on the method of Ref. 19. Our approach does not assume an overdamped limit and naturally preserves the quaternion unit length up to machine precision.

The rest of the paper is organised as follows. After introducing various quantities important for the problem setting in Section II, we present new Langevin-type equations for rigid body dynamics with HI in Section III. In Section IV, we derive a geometric integrator for the proposed Langevin-type equations, with the implementation described in Appendix B. In Section V we report results of a number of numerical experiments which test the constructed numerical method and also illustrate behaviour of the new Langevin model.

II. PRELIMINARIES

Consider a system of n rigid bodies with the centre-of-mass coordinates $\mathbf{r} = (r^1, \dots, r^n)^\top \in \mathbb{R}^{3n}$, $r^i = (r_1^i, r_2^i, r_3^i)^\top \in \mathbb{R}^3$ and orientations given by the unit quaternions $\mathbf{q} = (q^1, \dots, q^n)^\top$, $q^i = (q_0^i, q_1^i, q_2^i, q_3^i)^\top \in \mathbb{S}^3$, (i.e., $|q^i| = 1$), immersed in an incompressible Newtonian fluid with viscosity η . If the interaction between particles is specified by an effective potential energy function $U(\mathbf{r}, \mathbf{q})$, we can write a Hamiltonian for the n rigid bodies in the form (see Ref. 20):

$$H(\mathbf{r}, \mathbf{p}, \mathbf{q}, \boldsymbol{\pi}) = \sum_{i=1}^n \frac{p^i \cdot p^i}{2m_i} + \sum_{i=1}^n \sum_{l=1}^3 \frac{1}{I_l^i} V_l(q^i, \pi^i) + U(\mathbf{r}, \mathbf{q}), \quad (1)$$

where $\mathbf{p} = (p^1, \dots, p^n)^\top \in \mathbb{R}^{3n}$, $p^i = (p_1^i, p_2^i, p_3^i)^\top \in \mathbb{R}^3$, are the center-of-mass momenta conjugate to \mathbf{r} ; $\boldsymbol{\pi} = (\pi^1, \dots, \pi^n)^\top$, $\pi^i = (\pi_0^i, \pi_1^i, \pi_2^i, \pi_3^i)^\top$ are the angular momenta conjugate to \mathbf{q} such that $q^i \cdot \pi^i = 0$, i.e., $\pi^i \in T_{q^i}^* \mathbb{S}^3$ which is the cotangent space to \mathbb{S}^3 at q^i . The second term in (1) represents the rotational kinetic energy of the system with

$$V_l(q, \pi) = \frac{1}{8} [\pi^\top S_l q]^2, \quad l = 1, 2, 3, \quad (2)$$

where the three constant 4-by-4 matrices S_l are

$$S_1 = \begin{bmatrix} 0 & -1 & 0 & 0 \\ 1 & 0 & 0 & 0 \\ 0 & 0 & 0 & 1 \\ 0 & 0 & -1 & 0 \end{bmatrix}, \quad S_2 = \begin{bmatrix} 0 & 0 & -1 & 0 \\ 0 & 0 & 0 & -1 \\ 1 & 0 & 0 & 0 \\ 0 & 1 & 0 & 0 \end{bmatrix}$$

$$S_3 = \begin{bmatrix} 0 & 0 & 0 & -1 \\ 0 & 0 & 1 & 0 \\ 0 & -1 & 0 & 0 \\ 1 & 0 & 0 & 0 \end{bmatrix},$$

and I_l^i are the principal moments of inertia of the rigid particle. The Newtonian equations of motion of the system described by the Hamiltonian in Eq. (1), neglecting the influence of the solvent, are given by

$$\begin{aligned} \frac{dr^i}{dt} &= \frac{p^i}{m^i}, \\ \frac{dp^i}{dt} &= f^i(\mathbf{r}, \mathbf{q}), \\ \frac{dq^i}{dt} &= \frac{1}{4} \hat{S}(q^i) \hat{D}^i \hat{S}^\top(q^i) \pi^i, \\ \frac{d\pi^i}{dt} &= \frac{1}{4} \hat{S}(\pi^i) \hat{D}^i \hat{S}^\top(q^i) \pi^i + F^i(\mathbf{r}, \mathbf{q}), \end{aligned} \quad (3)$$

$i = 1, \dots, n$, where $f^i(\mathbf{r}, \mathbf{q}) = -\nabla_{r^i} U(\mathbf{r}, \mathbf{q}) \in \mathbb{R}^3$ is the translational force acting on particle i and $F^i(\mathbf{r}, \mathbf{q}) = -\tilde{\nabla}_{q^i} U(\mathbf{r}, \mathbf{q})$ is the rotational force. We also introduce a diagonal matrix $\hat{D}^i = \text{diag}(1/I_1^i, 1/I_2^i, 1/I_3^i)$ and a 4-by-3 matrix

$$\hat{S}(q) = [S_1 q, S_2 q, S_3 q] = \begin{bmatrix} -q_1 & -q_2 & -q_3 \\ q_0 & -q_3 & q_2 \\ q_3 & q_0 & -q_1 \\ -q_2 & q_1 & q_0 \end{bmatrix}. \quad (4)$$

Note that $q^\top \hat{S}(q) = (0, 0, 0)$ and $\hat{S}^\top(q) \hat{S}(q) = \mathbf{1}_3$.

We remark that, while ∇_x is the gradient in the Cartesian coordinates in \mathbb{R}^3 , $\tilde{\nabla}_q$ is the directional derivative tangent to the three-dimensional sphere \mathbb{S}^3 , implying that $q^i \cdot \tilde{\nabla}_q F^i = 0$. The directional derivative can be expressed in terms of the four-dimensional gradient as $\tilde{\nabla}_q = (\mathbf{1}_4 - qq^\top) \nabla_q$, where $\mathbf{1}_4$ is the four-dimensional identity matrix. The rotational force can also be calculated as $F^i = 2\hat{S}(q^i) \tau^i$, where $\tau^i \in \mathbb{R}^3$ is the torque on molecule i in the *body-fixed coordinate frame* (i.e. with axes aligned with the principal axes of the rigid body and rotating with it).

In addition to the interaction forces, the particles also experience drag forces due to their motion relative to the fluid and stochastic forces due to thermal fluctuations. In the low Reynolds number regime, the hydrodynamic force f_h^i and torque T_h^i experienced by particle i depend linearly on the linear and angular velocities, $v^i = p^i/m^i$ and Ω^i , through a $6n$ -by- $6n$ position-dependent *friction matrix*

$$\xi(\mathbf{r}, \mathbf{q}) = \begin{bmatrix} \text{tt}\xi(\mathbf{r}, \mathbf{q}) & \text{tr}\xi(\mathbf{r}, \mathbf{q}) \\ \text{rt}\xi(\mathbf{r}, \mathbf{q}) & \text{rr}\xi(\mathbf{r}, \mathbf{q}) \end{bmatrix}, \quad (5)$$

as follows

$$f_{\mathbf{h}}^i = - \sum_{j=1}^n \left({}^{\text{tt}}\xi^{(i,j)}(\mathbf{r}, \mathbf{q}) v^j + {}^{\text{tr}}\xi^{(i,j)}(\mathbf{r}, \mathbf{q}) \Omega^j \right), \quad (6)$$

$$T_{\mathbf{h}}^i = - \sum_{j=1}^n \left({}^{\text{rt}}\xi^{(i,j)}(\mathbf{r}, \mathbf{q}) v^j + {}^{\text{rr}}\xi^{(i,j)}(\mathbf{r}, \mathbf{q}) \Omega^j \right),$$

$$i = 1, \dots, n,$$

where $T_{\mathbf{h}}^i$ and Ω^i are torques and angular velocities in the *space-fixed coordinate frame*. The left superscripts t and r denote components of the friction matrix ξ coupling the translational and rotational degrees of freedom, respectively. Each sub-matrix ${}^{ab}\xi(\mathbf{r}, \mathbf{q})$ in Eq. (5) contains n^2 3-by-3 blocks ${}^{ab}\xi^{(i,j)}(\mathbf{r}, \mathbf{q})$, $i, j = 1, \dots, n$, $a, b = \text{t}, \text{r}$. Matrix $\xi(\mathbf{r}, \mathbf{q})$ is symmetric, so that ${}^{\text{tt}}\xi^{(i,j)} = {}^{\text{tt}}\xi^{(j,i)\text{T}}$, ${}^{\text{tr}}\xi^{(i,j)} = {}^{\text{rt}}\xi^{(j,i)\text{T}}$, and ${}^{\text{rr}}\xi^{(i,j)} = {}^{\text{rr}}\xi^{(j,i)\text{T}}$. The calculation of the friction matrix is, in general, a complex problem for which many approximate results exist¹. The best choice of a friction matrix for a given problem is beyond the scope of this paper – we simply present a method into which any well-defined positive-definite symmetric friction matrix ξ can be substituted. We note that in HI calculations one usually uses spherical particles as an approximation due to the difficulty in calculating hydrodynamic coupling for non-spherical particles. In the case of this approximation the friction matrix ξ depends only on the centre-of-mass positions \mathbf{r} . By including dependence of ξ on the orientation of particles expressed via quaternions \mathbf{q} , we allow for hydrodynamic interactions between non-spherical objects. One approach would be to model non-spherical particles as rigid clusters of spherical particles²¹ for the purposes of calculating ξ , in which case \mathbf{r} and \mathbf{q} would represent positions and orientations of the clusters.

The stochastic forces can be modelled by white noise, which, in the absence of any other external forces, ensures that the equilibrium probability distribution of the system is Gibbsian with temperature T : $\rho(\mathbf{r}, \mathbf{p}, \mathbf{q}, \boldsymbol{\pi}) \propto \exp(-\beta H(\mathbf{r}, \mathbf{p}, \mathbf{q}, \boldsymbol{\pi}))$, where $\beta^{-1} = k_B T$.

The angular velocity Ω^i in the space-fixed coordinate frame is related to the conjugate momentum π^i as follows

$$\Omega^i = A^{\text{T}}(q^i) \omega^i = \frac{1}{2} A^{\text{T}}(q^i) \hat{D}^i \hat{S}^{\text{T}}(q^i) \pi^i, \quad (7)$$

where ω^i is the angular velocity in the *body-fixed coordinate frame* (with coordinate axes aligned with the principal directions of the rigid body), and the rotation matrix,

$$A(q) = 2 \begin{bmatrix} q_0^2 + q_1^2 - \frac{1}{2} & q_1 q_2 + q_0 q_3 & q_1 q_3 - q_0 q_2 \\ q_1 q_2 - q_0 q_3 & q_0^2 + q_2^2 - \frac{1}{2} & q_2 q_3 + q_0 q_1 \\ q_1 q_3 + q_0 q_2 & q_2 q_3 - q_0 q_1 & q_0^2 + q_3^2 - \frac{1}{2} \end{bmatrix}, \quad (8)$$

transforms from space-fixed to body-fixed frame, while its transpose $A^{\text{T}}(q)$ transforms from body-fixed to space-fixed frame. For example, the torque τ^i on particle i in the body-fixed frame is related to the torque in the space-fixed frame T^i by $\tau^i = A(q^i) T^i$.

III. NEW LANGEVIN-TYPE EQUATIONS FOR RIGID BODY DYNAMICS WITH HYDRODYNAMIC INTERACTIONS

Based on Section II, the time evolution of rigid bodies under influence of conservative forces, hydrodynamic interactions and thermal noise can be modelled by the following Langevin-type equations (in the form of Itô):

$$dR^i = \frac{P^i}{m^i} dt, \quad R^i(0) = r^i, \quad (9)$$

$$dP^i = f^i(\mathbf{R}, \mathbf{Q}) dt - \sum_{j=1}^n {}^{\text{tt}}\xi^{(i,j)}(\mathbf{R}, \mathbf{Q}) \frac{P^j}{m^j} dt$$

$$- \frac{1}{2} \sum_{j=1}^n {}^{\text{tr}}\xi^{(i,j)}(\mathbf{R}, \mathbf{Q}) A^{\text{T}}(Q^j) \hat{D}^j \hat{S}^{\text{T}}(Q^j) \Pi^j dt$$

$$+ \sum_{j=1}^n {}^{\text{tb}}^{(i,j)}(\mathbf{R}, \mathbf{Q}) dw^j(t) + \sum_{j=1}^n {}^{\text{tr}}b^{(i,j)}(\mathbf{R}, \mathbf{Q}) dW^j(t),$$

$$P^i(0) = p^i,$$

$$dQ^i = \frac{1}{4} \hat{S}(Q^i) \hat{D}^i \hat{S}^{\text{T}}(Q^i) \Pi^i dt, \quad (10)$$

$$Q^i(0) = q^i, \quad |q^i| = 1,$$

$$d\Pi^i = \frac{1}{4} \hat{S}(\Pi^i) \hat{D}^i \hat{S}^{\text{T}}(Q^i) \Pi^i dt + F^i(\mathbf{R}, \mathbf{Q}) dt$$

$$- \sum_{j=1}^n \check{S}(Q^i) {}^{\text{rr}}\xi^{(i,j)}(\mathbf{R}, \mathbf{Q}) A^{\text{T}}(Q^j) \hat{D}^j \hat{S}^{\text{T}}(Q^j) \Pi^j dt$$

$$- 2 \sum_{j=1}^n \check{S}(Q^i) {}^{\text{rt}}\xi^{(i,j)}(\mathbf{R}, \mathbf{Q}) \frac{P^j}{m^j} dt$$

$$+ 2 \sum_{j=1}^n \check{S}(Q^i) {}^{\text{rr}}b^{(i,j)}(\mathbf{R}, \mathbf{Q}) dW^j(t)$$

$$+ 2 \sum_{j=1}^n \check{S}(Q^i) {}^{\text{rt}}b^{(i,j)}(\mathbf{R}, \mathbf{Q}) dw^j(t),$$

$$\Pi^i(0) = \pi^i, \quad q^{i\text{T}} \pi^i = 0, \quad i = 1, \dots, n,$$

where ${}^{\text{tb}}^{(i,j)}(\mathbf{r}, \mathbf{q})$, ${}^{\text{tr}}b^{(i,j)}(\mathbf{r}, \mathbf{q})$, ${}^{\text{rr}}b^{(i,j)}(\mathbf{r}, \mathbf{q})$, and ${}^{\text{rt}}b^{(i,j)}(\mathbf{r}, \mathbf{q})$ are 3×3 -matrices; $(\mathbf{w}^{\text{T}}, \mathbf{W}^{\text{T}})^{\text{T}} = (w_1^{\text{T}}, \dots, w_n^{\text{T}}, W_1^{\text{T}}, \dots, W_n^{\text{T}})^{\text{T}}$ is a $(3n + 3n)$ -dimensional standard Wiener process with $w^i = (w_1^i, w_2^i, w_3^i)^{\text{T}}$ and $W^i = (W_1^i, W_2^i, W_3^i)^{\text{T}}$. We also define

$$\check{S}(q) = \hat{S}(q) A(q) = \begin{bmatrix} -q_1 & -q_2 & -q_3 \\ q_0 & q_3 & -q_2 \\ -q_3 & q_0 & q_1 \\ q_2 & -q_1 & q_0 \end{bmatrix} \quad (11)$$

given that $|q| = 1$. Note that $q^{\text{T}} \check{S}(q) = (0, 0, 0)$, $\check{S}^{\text{T}}(q) \check{S}(q) = \mathbf{1}_3$, and $A(q) = \hat{S}^{\text{T}}(q) \check{S}(q)$.

The Langevin model (9)-(10) has the following properties:

1. The solution of (9)-(10) preserves the quaternion lengths:

$$|Q^i(t)| = 1, \quad i = 1, \dots, n, \quad \text{for all } t \geq 0. \quad (12)$$

2. The solution of (9)-(10) preserves orthogonality of $\mathbf{Q}(t)$ and $\mathbf{\Pi}(t)$:

$$\mathbf{Q}^\top(t)\mathbf{\Pi}(t) = 0, \quad \text{for all } t \geq 0. \quad (13)$$

3. The Itô interpretation of the system of SDEs (9)-(10) coincides with its Stratonovich interpretation.

4. Assume that the solution $X(t) = (\mathbf{R}^\top(t), \mathbf{P}^\top(t), \mathbf{Q}^\top(t), \mathbf{\Pi}^\top(t))^\top$ of (9)-(10) is an ergodic process^{22,23} on

$$\mathbb{D} = \{x = (\mathbf{r}^\top, \mathbf{p}^\top, \mathbf{q}^\top, \boldsymbol{\pi}^\top)^\top \in \mathbb{R}^{14n} : |q^i| = 1, (q^i)^\top \pi^i = 0, \quad i = 1, \dots, n\}.$$

Then the invariant measure of $X(t)$ is Gibbsian with the density $\rho(\mathbf{r}, \mathbf{p}, \mathbf{q}, \boldsymbol{\pi})$,

$$\rho(\mathbf{r}, \mathbf{p}, \mathbf{q}, \boldsymbol{\pi}) \propto \exp(-\beta H(\mathbf{r}, \mathbf{p}, \mathbf{q}, \boldsymbol{\pi})), \quad (14)$$

if the following condition holds

$$b(\mathbf{r}, \mathbf{q})b^\top(\mathbf{r}, \mathbf{q}) = \frac{2}{\beta} \xi(\mathbf{r}, \mathbf{q}), \quad (15)$$

where

$$b(\mathbf{r}, \mathbf{q}) = \begin{bmatrix} {}^{\text{tt}}b(\mathbf{r}, \mathbf{q}) & {}^{\text{tr}}b(\mathbf{r}, \mathbf{q}) \\ {}^{\text{rt}}b(\mathbf{r}, \mathbf{q}) & {}^{\text{rr}}b(\mathbf{r}, \mathbf{q}) \end{bmatrix} \quad (16)$$

and each sub-matrix ${}^{ab}b(\mathbf{r}, \mathbf{q})$ contains n^2 3-by-3 blocks ${}^{ab}b^{(i,j)}(\mathbf{r}, \mathbf{q})$, $i, j = 1, \dots, n$, $a, b = \text{t}, \text{r}$.

This last property can be demonstrated by verifying that the stationary Fokker-Planck equation corresponding to (9)-(10) is satisfied with ρ given by Eq. (14) and H by Eq. (1).

We note that if ${}^{\text{tr}}\xi^{(i,j)} = {}^{\text{rt}}\xi^{(j,i)} = 0$, ${}^{\text{tr}}b^{(i,j)} = {}^{\text{rt}}b^{(j,i)} = 0$, and ${}^{\text{tt}}\xi^{(i,j)}$, ${}^{\text{rr}}\xi^{(i,j)}$, ${}^{\text{tt}}b^{(i,j)}$, and ${}^{\text{rr}}b^{(i,j)}$ are appropriately chosen diagonal constant matrices, then the system (9)-(10) degenerates to the Langevin thermostat for rigid bodies from Ref. 19.

The Langevin system (9)-(10) is driven by the conservative forces, hydrodynamic interactions and thermal noise. It is worthwhile (see e.g. Refs. 24–26 and the example in Section V D here) to generalize this system by including non-conservative, possibly time-dependent, forces $\tilde{\mathbf{f}}(t, \mathbf{r}, \mathbf{q})$ and $\tilde{\mathbf{F}}(t, \mathbf{r}, \mathbf{q})$, i.e., to consider the follow-

ing system of Langevin-type equations:

$$dR^i = \frac{P^i}{m^i} dt, \quad R^i(0) = r^i, \quad (17)$$

$$dP^i = f^i(\mathbf{R}, \mathbf{Q})dt + \tilde{f}^i(t, \mathbf{R}, \mathbf{Q})dt - \sum_{j=1}^n {}^{\text{tt}}\xi^{(i,j)}(\mathbf{R}, \mathbf{Q}) \frac{P^j}{m^j} dt - \frac{1}{2} \sum_{j=1}^n {}^{\text{tr}}\xi^{(i,j)}(\mathbf{R}, \mathbf{Q}) A^\top(Q^j) \hat{D}^j \hat{S}^\top(Q^j) \Pi^j dt + \sum_{j=1}^n {}^{\text{tr}}b^{(i,j)}(\mathbf{R}, \mathbf{Q}) dw^j(t) + \sum_{j=1}^n {}^{\text{tr}}b^{(i,j)}(\mathbf{R}, \mathbf{Q}) dW^j(t), \quad P^i(0) = p^i,$$

$$dQ^i = \frac{1}{4} \hat{S}(Q^i) \hat{D}^i \hat{S}^\top(Q^i) \Pi^i dt, \quad (18)$$

$$Q^i(0) = q^i, \quad |q^i| = 1,$$

$$d\Pi^i = \frac{1}{4} \hat{S}(\Pi^i) \hat{D}^i \hat{S}^\top(Q^i) \Pi^i dt + F^i(\mathbf{R}, \mathbf{Q})dt + \tilde{F}^i(t, \mathbf{R}, \mathbf{Q})dt - \sum_{j=1}^n \check{S}(Q^i) {}^{\text{rr}}\xi^{(i,j)}(\mathbf{R}, \mathbf{Q}) A^\top(Q^j) \hat{D}^j \hat{S}^\top(Q^j) \Pi^j dt - 2 \sum_{j=1}^n \check{S}(Q^i) {}^{\text{rt}}\xi^{(i,j)}(\mathbf{R}, \mathbf{Q}) \frac{P^j}{m^j} dt + 2 \sum_{j=1}^n \check{S}(Q^i) {}^{\text{rr}}b^{(i,j)}(\mathbf{R}, \mathbf{Q}) dW^j(t) + 2 \sum_{j=1}^n \check{S}(Q^i) {}^{\text{rt}}b^{(i,j)}(\mathbf{R}, \mathbf{Q}) dw^j(t), \quad \Pi^i(0) = \pi^i, \quad q^{i\top} \pi^i = 0, \quad i = 1, \dots, n,$$

where $\mathbf{q}^\top \tilde{\mathbf{F}}(t, \mathbf{r}, \mathbf{q}) = 0$. The first three properties stated above for the model (9)-(10) are also true for the system (17)-(18).

IV. NUMERICAL INTEGRATOR

We propose a weak 2nd order numerical integrator for (9)-(10), which is a generalization of the Langevin C method in Ref. 19. The new integrator is based on splitting (9)-(10) into the deterministic Hamiltonian system

(3) and the Ornstein-Uhlenbeck-type SDEs

$$\begin{aligned}
dP^i &= - \sum_{j=1}^n \text{tt} \xi^{(i,j)}(\mathbf{r}, \mathbf{q}) \frac{P^j}{m^j} dt \\
&\quad - \frac{1}{2} \sum_{j=1}^n \text{tr} \xi^{(i,j)}(\mathbf{r}, \mathbf{q}) A^\top(q^j) \hat{D}^j \hat{S}^\top(q^j) \Pi^j dt \\
&\quad + \sum_{j=1}^n \text{tt} b^{(i,j)}(\mathbf{r}, \mathbf{q}) dw^j(t) + \sum_{j=1}^n \text{tr} b^{(i,j)}(\mathbf{r}, \mathbf{q}) dW^j(t), \\
d\Pi^i &= - \sum_{j=1}^n \check{S}(q^i)^{\text{rr}} \xi^{(i,j)}(\mathbf{r}, \mathbf{q}) A^\top(q^j) \hat{D}^j \hat{S}^\top(q^j) \Pi^j dt \\
&\quad - 2 \sum_{j=1}^n \check{S}(q^i)^{\text{rt}} \xi^{(i,j)}(\mathbf{r}, \mathbf{q}) \frac{P^j}{m^j} dt \\
&\quad + 2 \sum_{j=1}^n \check{S}(q^i)^{\text{rr}} b^{(i,j)}(\mathbf{r}, \mathbf{q}) dW^j(t) \\
&\quad + 2 \sum_{j=1}^n \check{S}(q^i)^{\text{rt}} b^{(i,j)}(\mathbf{r}, \mathbf{q}) dw^j(t),
\end{aligned} \tag{19}$$

where \mathbf{r} and \mathbf{q} are fixed. Let us re-write (19) in a more compact form. Using the notation

$$\begin{aligned}
\text{tt} \tilde{\xi}^{(i,j)}(\mathbf{r}, \mathbf{q}) &:= \frac{1}{m^j} \text{tt} \xi^{(i,j)}(\mathbf{r}, \mathbf{q}), \\
\text{tr} \tilde{\xi}^{(i,j)}(\mathbf{r}, \mathbf{q}) &:= \frac{1}{2} \text{tr} \xi^{(i,j)}(\mathbf{r}, \mathbf{q}) A^\top(q^j) \hat{D}^j \hat{S}^\top(q^j), \\
\text{rt} \tilde{\xi}^{(i,j)}(\mathbf{r}, \mathbf{q}) &:= \frac{2}{m^j} \check{S}(q^i)^{\text{rt}} \xi^{(i,j)}(\mathbf{r}, \mathbf{q}), \\
\text{rr} \tilde{\xi}^{(i,j)}(\mathbf{r}, \mathbf{q}) &:= \check{S}(q^i)^{\text{rr}} \xi^{(i,j)}(\mathbf{r}, \mathbf{q}) A^\top(q^j) \hat{D}^j \hat{S}^\top(q^j), \\
\text{rr} \tilde{b}^{(i,j)}(\mathbf{r}, \mathbf{q}) &:= 2 \check{S}(q^i)^{\text{rr}} b^{(i,j)}(\mathbf{r}, \mathbf{q}), \\
\text{rt} \tilde{b}^{(i,j)}(\mathbf{r}, \mathbf{q}) &:= 2 \check{S}(q^i)^{\text{rt}} b^{(i,j)}(\mathbf{r}, \mathbf{q}), \\
\text{tt} \tilde{b}^{(i,j)}(\mathbf{r}, \mathbf{q}) &:= \text{tt} b^{(i,j)}(\mathbf{r}, \mathbf{q}), \\
\text{rr} \tilde{b}^{(i,j)}(\mathbf{r}, \mathbf{q}) &:= \text{rr} b^{(i,j)}(\mathbf{r}, \mathbf{q}),
\end{aligned} \tag{20}$$

we can write (19) in the form

$$\begin{aligned}
d\mathbf{P} &= - \text{tt} \tilde{\xi}(\mathbf{r}, \mathbf{q}) \mathbf{P} dt - \text{tr} \tilde{\xi}(\mathbf{r}, \mathbf{q}) \mathbf{\Pi} dt \\
&\quad + \text{tt} \tilde{b}(\mathbf{r}, \mathbf{q}) d\mathbf{w}(t) + \text{tr} \tilde{b}(\mathbf{r}, \mathbf{q}) d\mathbf{W}(t), \\
d\mathbf{\Pi} &= - \text{rr} \tilde{\xi}(\mathbf{r}, \mathbf{q}) \mathbf{\Pi} dt - \text{rt} \tilde{\xi}(\mathbf{r}, \mathbf{q}) \mathbf{P} dt \\
&\quad + \text{rt} \tilde{b}(\mathbf{r}, \mathbf{q}) d\mathbf{w}(t) + \text{rr} \tilde{b}(\mathbf{r}, \mathbf{q}) d\mathbf{W}(t),
\end{aligned} \tag{21}$$

which we can combine as

$$dY = -\tilde{\xi}(\mathbf{r}, \mathbf{q}) Y + \tilde{b}(\mathbf{r}, \mathbf{q}) d\tilde{\mathbf{W}}(t), \tag{22}$$

where

$$\begin{aligned}
\tilde{\xi}(\mathbf{r}, \mathbf{q}) &:= \begin{bmatrix} \text{tt} \tilde{\xi}(\mathbf{r}, \mathbf{q}) & \text{tr} \tilde{\xi}(\mathbf{r}, \mathbf{q}) \\ \text{rt} \tilde{\xi}(\mathbf{r}, \mathbf{q}) & \text{rr} \tilde{\xi}(\mathbf{r}, \mathbf{q}) \end{bmatrix}, \\
\tilde{b}(\mathbf{r}, \mathbf{q}) &:= \begin{bmatrix} \text{tt} \tilde{b}(\mathbf{r}, \mathbf{q}) & \text{tr} \tilde{b}(\mathbf{r}, \mathbf{q}) \\ \text{rt} \tilde{b}(\mathbf{r}, \mathbf{q}) & \text{rr} \tilde{b}(\mathbf{r}, \mathbf{q}) \end{bmatrix}, \\
Y &:= \begin{bmatrix} \mathbf{P} \\ \mathbf{\Pi} \end{bmatrix}, \quad \tilde{\mathbf{W}}(t) := \begin{bmatrix} \mathbf{w}(t) \\ \mathbf{W}(t) \end{bmatrix}.
\end{aligned}$$

Note that, unlike $\xi(\mathbf{r}, \mathbf{q})$, the matrix $\tilde{\xi}(\mathbf{r}, \mathbf{q})$ is not symmetric.

The solution of the linear SDEs with additive noise (22) is given by

$$Y(t) = e^{-\tilde{\xi}(\mathbf{r}, \mathbf{q})t} Y(0) + \int_0^t e^{-\tilde{\xi}(\mathbf{r}, \mathbf{q})(t-s)} \tilde{b}(\mathbf{r}, \mathbf{q}) d\tilde{\mathbf{W}}(s). \tag{23}$$

The $7n$ -dimensional vector $\int_0^t e^{-\tilde{\xi}(\mathbf{r}, \mathbf{q})(t-s)} \tilde{b}(\mathbf{r}, \mathbf{q}) d\tilde{\mathbf{W}}(t)$ is Gaussian with zero mean and covariance

$$C(t; \mathbf{r}, \mathbf{q}) = \int_0^t e^{-\tilde{\xi}(\mathbf{r}, \mathbf{q})(t-s)} \tilde{b}(\mathbf{r}, \mathbf{q}) \tilde{b}^\top(\mathbf{r}, \mathbf{q}) e^{-\tilde{\xi}^\top(\mathbf{r}, \mathbf{q})(t-s)} ds. \tag{24}$$

Introducing a $7n$ -by- $6n$ matrix $\sigma(t; \mathbf{r}, \mathbf{q})$ such that

$$\sigma(t; \mathbf{r}, \mathbf{q}) \sigma^\top(t; \mathbf{r}, \mathbf{q}) = C(t; \mathbf{r}, \mathbf{q}), \tag{25}$$

we can write Eq. (23) in the form

$$Y(t) = e^{-\tilde{\xi}(\mathbf{r}, \mathbf{q})t} Y(0) + \sigma(t; \mathbf{r}, \mathbf{q}) \chi, \tag{26}$$

where χ is a $6n$ -dimensional vector consisting of independent Gaussian random variables with zero mean and unit variance. Details of the evaluation of the covariance integral (24) and matrix $\sigma(t; \mathbf{r}, \mathbf{q})$ can be found in the Appendix A.

Starting from the initial conditions $\mathbf{P}_0 = \mathbf{p}$, $\mathbf{R}_0 = \mathbf{r}$, $\mathbf{Q}_0 = \mathbf{q}$, $|q^i| = 1$, $i = 1, \dots, n$, $\mathbf{\Pi}_0 = \boldsymbol{\pi}$, $\mathbf{q}^\top \boldsymbol{\pi} = 0$, the numerical integrator for (9)-(10) with stepsize h takes the form

$$\mathcal{P}_{1,k}^i = P_k^i + \frac{h}{2} f^i(\mathbf{R}_k, \mathbf{Q}_k), \tag{27}$$

$$\Pi_{1,k}^i = \Pi_k^i + \frac{h}{2} F^i(\mathbf{R}_k, \mathbf{Q}_k),$$

$$\mathcal{R}_{1,k}^i = R_k^i + \frac{h}{2} \frac{\mathcal{P}_{1,k}^i}{m^i},$$

$$(\mathcal{Q}_{1,k}^i, \Pi_{2,k}^i) = \Psi_{h/2}^-(\mathcal{Q}_k^i, \Pi_{1,k}^i),$$

$$\begin{bmatrix} \mathcal{P}_{2,k} \\ \Pi_{3,k} \end{bmatrix} = e^{-\tilde{\xi}(\mathcal{R}_{1,k}, \mathcal{Q}_{1,k})h} \begin{bmatrix} \mathcal{P}_{1,k} \\ \Pi_{2,k} \end{bmatrix} + \sigma(h; \mathcal{R}_{1,k}, \mathcal{Q}_{1,k}) \chi_k,$$

$$R_{k+1}^i = \mathcal{R}_{1,k}^i + \frac{h}{2} \frac{\mathcal{P}_{2,k}^i}{m^i},$$

$$(\mathcal{Q}_{k+1}^i, \Pi_{4,k}^i) = \Psi_{h/2}^+(\mathcal{Q}_{1,k}^i, \Pi_{3,k}^i),$$

$$P_{k+1}^i = \mathcal{P}_{2,k}^i + \frac{h}{2} f^i(\mathbf{R}_{k+1}, \mathbf{Q}_{k+1}),$$

$$\Pi_{k+1}^i = \Pi_{4,k}^i + \frac{h}{2} F^i(\mathbf{R}_{k+1}, \mathbf{Q}_{k+1}),$$

$i = 1, \dots, n$, where χ_k is a $6n$ -dimensional vector with components being i.i.d. Gaussian random variables with zero mean and unit variance $\mathcal{N}(0, 1)$. We note in passing that for weak convergence it is sufficient²⁷ to use the simple law: $P(\theta = 0) = 2/3$, $P(\theta = \pm\sqrt{3}) = 1/6$ for the components of χ_k .

As in Ref. 19 (see also Refs. 17 and 20), we use exact rotations around each principal axis written as the maps

$\Psi_{t,l}(q, \pi) : (q, \pi) \mapsto (Q, \Pi)$ defined by:

$$\begin{aligned} Q &= \cos(\zeta_l t)q + \sin(\zeta_l t)S_l q, \\ \Pi &= \cos(\zeta_l t)\pi + \sin(\zeta_l t)S_l \pi, \end{aligned} \quad (28)$$

where $\zeta_l = \frac{1}{4I_l} \pi^\top S_l q$. Based on (28), the composite maps $\Psi_{t,l}^\pm(q, \pi) : (q, \pi) \mapsto (Q, \Pi)$ used in (27) are defined as

$$\begin{aligned} \Psi_t^- &= \Psi_{t,3} \circ \Psi_{t,2} \circ \Psi_{t,1}, \\ \Psi_t^+ &= \Psi_{t,1} \circ \Psi_{t,2} \circ \Psi_{t,3}, \end{aligned} \quad (29)$$

where “ \circ ” denotes function composition, i.e., $(g \circ f)(x) = g(f(x))$. Implementation details for the method (27) are given in Appendix B.

The proposed method (27) has the following properties:

- it is quasi-symplectic, in the sense that it degenerates to Langevin C from Ref. 19 (see also Refs. 27 and 28);
- it preserves $|Q_k^j| = 1$, $j = 1, \dots, n$, for all $t_k \geq 0$ automatically;
- it preserves $Q_k^{j\top} \Pi_k^j = 0$, $j = 1, \dots, n$, for $t_k \geq 0$ automatically;
- only a single evaluation of forces and the friction matrix per step is required;
- it is of weak order 2.

The weak convergence of the method is proved by the standard arguments as follows. We apply the one-step approximation corresponding to the standard weak-second-order Taylor-type method from Ref. 27, p. 94 to the SDEs (9)-(10) and compare it with an appropriate expansion of the one-step approximation corresponding to the method (27). This comparison together with the general weak convergence theorem (see Ref. 27, pp.100-101) confirms weak 2nd order of (27).

Remark IV.1 *In Ref. 19 we constructed three weak 2nd order geometric integrators (Langevin A, B and C) for a Langevin thermostat (without HI). The integrators were derived using different splittings of the flow of the continuous Langevin dynamics. In our previous numerical tests¹⁹ we identified that Langevin A and C are more accurate than Langevin B in computing configurational quantities. It was then natural to try to generalise Langevin A and C to the case considered here, the SDEs (9)-(10). Using the same splitting as for Langevin C in Ref. 19, we have succeeded in constructing the presented above method (27) with the desirable properties, in particular that it is of second weak order. However, an attempt to generalize Langevin A failed, which is an interesting observation from the point of view of stochastic geometric integration.*

We recall²⁷ that weak-sense numerical methods for SDEs are sufficient for approximating expectations of the SDEs solutions, such as those considered in examples of Sections V B and V C. When one aims to visualize individual trajectories of SDEs solutions (e.g., as in the example of Section V D), then mean-square (strong-sense) approximations are needed as they can ensure closeness of an approximate trajectory to the corresponding exact trajectory²⁷. The proposed method (27) with random variables involved being simulated as $\mathcal{N}(0, 1)$ is of mean-square order one, which is proved by comparing (27) with the mean-square Euler scheme and by applying the fundamental mean-square convergence theorem²⁷. We also note that often, as in the example of Section V D, the noise intensity is small. If we denote by ε the parameter characterizing smallness of noise in (9)-(10), then the mean-square accuracy of the method (27) with random variables simulated as $\mathcal{N}(0, 1)$ is $O(h^2 + \varepsilon h)$. The corresponding proof rests on the results from Ref. 29 (see also Ref. 27, Chapter 3).

We point out, however, that even in the dynamical context we are not primarily concerned with the behaviour of individual trajectories³. Nonlinearities lead to an exponential divergence of trajectories from those obtained in the $h \rightarrow 0$ limit, and it is infeasible to compare individual trajectories directly with experiment due to a sensitive dependence on initial conditions³. Instead, we are primarily interested in statistical properties of trajectories, for which expectations are more relevant. Thus, the main practical interest is in weak convergence and weak-sense approximations.

Remark IV.2 *To approximate the model (17)-(18) with time-dependent non-conservative forces, replace in (27):*

- $\mathbf{f}(\mathbf{R}_k, \mathbf{Q}_k)$ by $\mathbf{f}(\mathbf{R}_k, \mathbf{Q}_k) + \tilde{\mathbf{f}}(t_k, \mathbf{R}_k, \mathbf{Q}_k)$;
- $F^j(\mathbf{R}_k, \mathbf{Q}_k)$ by $F^j(\mathbf{R}_k, \mathbf{Q}_k) + \tilde{F}^j(t_k, \mathbf{R}_k, \mathbf{Q}_k)$;
- $\mathbf{f}(\mathbf{R}_{k+1}, \mathbf{Q}_{k+1})$ by $\mathbf{f}(\mathbf{R}_{k+1}, \mathbf{Q}_{k+1}) + \tilde{\mathbf{f}}(t_{k+1}, \mathbf{R}_{k+1}, \mathbf{Q}_{k+1})$;
- $F^j(\mathbf{R}_{k+1}, \mathbf{Q}_{k+1})$ by $F^j(\mathbf{R}_{k+1}, \mathbf{Q}_{k+1}) + \tilde{F}^j(t_{k+1}, \mathbf{R}_{k+1}, \mathbf{Q}_{k+1})$.

The resulting method for (17)-(18) is again of weak order 2 and of mean-square order 1.

V. NUMERICAL EXPERIMENTS

We perform four sets of numerical experiments. First, in Section V A, we demonstrate that the integrator without noise (i.e., $T = 0$) correctly converges to known analytical results for the dynamical properties of two sedimenting spheres. Then, in Section V B, we consider Lennard-Jones spheres under periodic boundary conditions, where the main aim is to test convergence and accuracy of the constructed geometric integrator with regard to its sampling from the canonical ensemble at

a given temperature $T > 0$. In Section VC we experiment with two spheres trapped in translational and rotational harmonic wells, and in Section VD we study circling spheres driven by external non-conservative force and torque.

In all numerical experiments, the HYDROLIB package³⁰ is used to calculate the hydrodynamic friction tensor $\xi(\mathbf{r})$. It allows the calculation of HI in systems of equal radius spheres without boundaries (as in experiments described in Sections VA, VC, and VD) or with periodic boundary conditions (as in Section VB). The calculations are based on a multipole expansion³¹ up to an order specified by integer parameter l_{\max} , which can take values between 0 and 3. We use $l_{\max} = 2$ in our calculations. Among other options available in HYDROLIB, we enable short-range corrections calculated from lubrication theory and use double-precision option for all external library functions.

A. Asymptotic motion of two sedimenting spheres

Before testing the performance of the numerical integrator (27) for the Langevin thermostat at finite temperature, we verify our use of HYDROLIB for computing HI and integration of the corresponding equations of motion in the noiseless regime (i.e., temperature $T = 0$). To this end, we compare our simulations to analytic results for the dynamics of two sedimenting spheres.

Analytic results for the dynamics of hydrodynamically-coupled rigid bodies are rare due to the inherent complexity of such systems. However, they exist for two spheres of radius a separated by distance l along the x axis, undergoing sedimentation parallel to the z -axis (pointing down) due to gravity and without noise³². Hydrodynamic coupling increases the sedimentation velocity and leads to rotation of the spheres.

Taking the sphere coordinates as $(-l/2, 0, 0)^T$ and $(l/2, 0, 0)^T$, and the gravitational force as $(0, 0, F)^T$ on both spheres, Happel and Brenner³² provide expansions in powers of a/l for the asymptotic velocity $(0, 0, U)^T$ of both spheres, and angular velocities $(0, -\omega, 0)^T$ and $(0, \omega, 0)^T$, respectively (see Eqs. (6-3.97) and (6-3.100) in Ref. 32):

$$F = 6\pi\eta aU \left(1 - \frac{3a}{4l} + \frac{9a^2}{16l^2} - \frac{59a^3}{64l^3} + \frac{273a^4}{256l^4} - \frac{1107a^5}{1024l^5} \right), \quad (30)$$

$$\omega = \frac{U}{a} \left(\frac{3a^2}{4l^2} - \frac{9a^3}{16l^3} + \frac{27a^4}{64l^4} - \frac{177a^5}{256l^5} + \frac{819a^6}{1024l^6} \right), \quad (31)$$

where η is the absolute fluid viscosity.

The following reduced units are imposed by the HYDROLIB package: the radius of the spheres is set to 1, the viscosity of the surrounding fluid η is set to $1/(4\pi)$.

TABLE I. Table of F/U and ω/U demonstrating good agreement between numerics (num) and theory (th) for sedimenting spheres, particularly for a large value of the ratio of sphere separation to radius, l/a .

l/a	$F/U(\text{num})$	$F/U(\text{th})$	$\omega/U(\text{num})$	$\omega/U(\text{th})$
10	1.3946988	1.3946984	0.006973076	0.006973573
4	1.2551892	1.2545428	0.03906680	0.03925395
3	1.1840827	1.1806098	0.06455729	0.06596017
5/2	1.1308965	1.1208450	0.08549728	0.09099600
25/12	1.0756197	1.0450674	0.09772490	0.12515166

In addition, the energy scale is set by choosing the force $F = 1.0$. We simulated sedimenting spheres using $m = 0.25$, $I = (0.1, 0.1, 0.1)$, $l = 10, 4, 3, 5/2$, and $25/12$, and time steps $h = 0.001, 0.01, 0.02, 0.03$, and 0.04 in these reduced units. As expected for a 2-nd order numerical integrator, we observed linear dependence of the computed results on h^2 . A linear fit of F/U and ω/U against h^2 was used to extrapolate the results to $h = 0$, and these results are compared to the predictions of Eqs. (30) and (31) in Table I. We see excellent agreement for large l/a , with the discrepancy increasing with decreasing l/a due to the truncation of both the theoretical expression and the multipole expansion approximation in HYDROLIB.

B. Lennard-Jones spheres in periodic boundary conditions

Having tested the implementation of HI in the noiseless limit, we now establish that the method converges to the correct Gibbsian distribution for a non-trivial model. We perform simulation of N interacting spheres in a cubic simulation box of size L with periodic boundary conditions (PBC). In addition to the HI evaluated in HYDROLIB with enabled PBC option, the spheres interact with one another via a pairwise smoothly truncated Lennard-Jones (LJ) potential

$$u(x) = \begin{cases} u_{\text{LJ}}(x), & x \leq x_m, \\ u_{\text{LJ}}(x)\phi(z(x)), & x_m < x < x_c, \\ 0, & x_c \leq x, \end{cases} \quad (32)$$

where $u_{\text{LJ}}(x) = 4\epsilon [(\sigma/x)^{12} - (\sigma/x)^6]$, $\phi(z) = 1 - 10z^3 + 15z^4 - 6z^5$, $z(x) = (x^2 - x_m^2)/(x_c^2 - x_m^2)$. The potential $u(x)$ is twice continuously differentiable. Here, x is the distance between interaction sites; the interaction site of sphere i is offset from the sphere centre-of-mass r^i by a vector d in the body frame, in order to induce rotational forces. We set the size of the box L sufficiently large so that $x_c \leq L/2$ and the minimum image convention applies. As such, the total potential energy of the spheres is

$$U(\mathbf{r}, \mathbf{q}) = \sum_{i=2}^N \sum_{j=1}^{i-1} u(|r^i + A^\top(q^i)d - r^j - A^\top(q^j)d|), \quad (33)$$

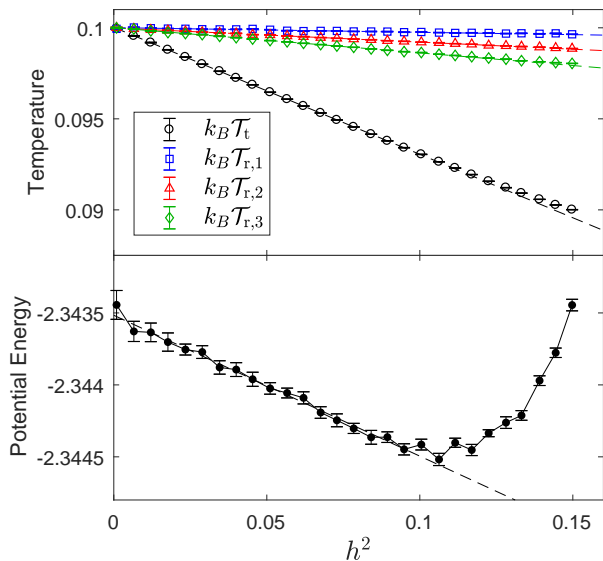


FIG. 1. Spheres in PBC with LJ and hydrodynamic interactions. $N = 8$, $k_B T = 0.1$. Dashed lines indicate straight line weighted least-squares approximation of the results for $h^2 < 0.1$.

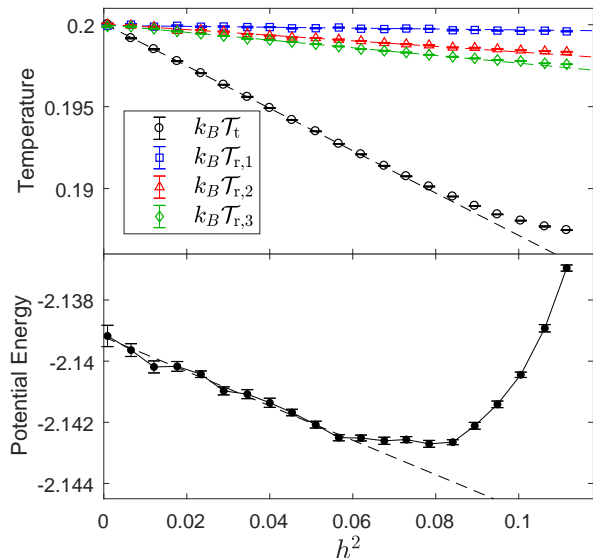


FIG. 2. Spheres in PBC with LJ and hydrodynamic interactions. Here $N = 8$ and $k_B T = 0.2$. Dashed lines indicate straight line weighted least-squares approximation of the results for $h^2 < 0.06$.

where q^i are the quaternion coordinates of sphere i .

We augment the reduced units of the HYDROLIB package (the radius of the spheres is set to 1, the viscosity of the surrounding fluid η is set to $1/(4\pi)$) with an energy scale by setting $\epsilon = 1$ in the Lennard-Jones potential. The values of all other parameters and measured results are reported in these reduced units.

TABLE II. Table of coefficients of least-square fit to the data at $h^2 < 0.1$ for $k_B T = 0.1$ and $h^2 < 0.06$ for $k_B T = 0.2$.

A	$k_B T = 0.1$		$k_B T = 0.2$	
	A_0	E_A	A_0	E_A
$k_B T_t$	0.100012(14)	-0.06972(11)	0.20001(2)	-0.1293(5)
$k_B T_{r,1}$	0.100010(18)	-0.00257(15)	0.19998(3)	-0.0027(7)
$k_B T_{r,2}$	0.099992(14)	-0.00778(12)	0.20002(2)	-0.0171(6)
$k_B T_{r,3}$	0.100011(12)	-0.01388(11)	0.19999(3)	-0.0235(5)
\mathcal{U}	-2.34352(3)	-0.0098(4)	-2.13921(14)	-0.056(3)

The numerical experiments were carried out with the following parameters: $N = 8$, $L = 15.0$, $\sigma = 2.6$. The mass of the spheres is $m = 5.0$, the principal moments of inertia are $I = (3.0, 2.0, 1.5)$, and $d = (0.2, 0.15, 0)^\top$. The LJ cut-off radius is $x_c = 2.5\sigma$, and $x_m = 0.9x_c$.

Simulations were carried out at temperatures $k_B T = 0.1$ and 0.2 , and a range of time steps h . After 2000 equilibration steps, the measurements were taken over 2×10^5 steps. 40 independent runs were performed at each h . We measure temperature from kinetic energy of the spheres, separately for translational and rotational degrees of freedom (separately for each $l = 1, 2, 3$):

$$\langle \mathcal{T}_t \rangle_h = \frac{\langle \mathbf{p}^\top \mathbf{p} \rangle_h}{3Nmk_B}, \quad (34)$$

$$\langle \mathcal{T}_{r,l} \rangle_h = \frac{2 \langle \sum_{j=1}^N V_l(q^j, \pi^j) \rangle_h}{Nk_B}, \quad (35)$$

as well as potential energy per sphere

$$\langle \mathcal{U} \rangle_h = \frac{1}{N} \langle U \rangle_h. \quad (36)$$

The results are shown in Figures 1 and 2, where we see convergence of both translational and rotational temperatures to the thermostat parameter when $h \rightarrow 0$. We observe linear dependence on h^2 for all measured quantities, as expected for a weak 2nd-order numerical integrator²⁷:

$$\langle A \rangle_h = A_0 + E_A h^2 + \mathcal{O}(h^3), \quad (37)$$

Estimated values of A_0 and E_A for the measured quantities are shown in Table II.

Even though the proposed integrator preserves the constraints $|q^i|^2 - 1 = 0$ and $q^{i\top} \pi^i = 0$, in practice these quantities gradually deviate from zero in the course of a long simulation due to the finite accuracy of double precision arithmetic. In our simulations we observe that starting with a deviation of the order of 10^{-16} in the double-precision computations, the maximum deviation grows to about 10^{-12} at the end of the simulation run, independent of the time step h . As we demonstrated in Ref. 19, the deviation of $q^{i\top} \pi^i$ from zero does not have any effect on physically relevant quantities. On the other hand, the deviation of $|q^i|^2$ from 1 does have an effect on

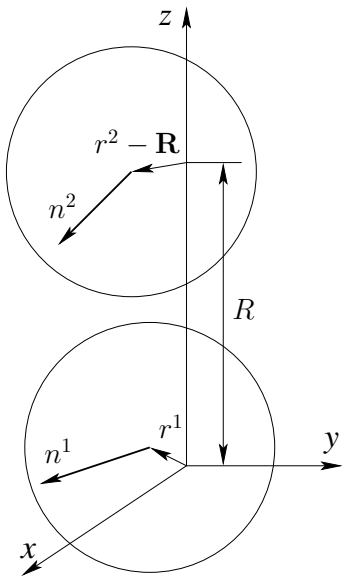


FIG. 3. Two harmonically trapped spheres.

measured quantities. Therefore, we recommend to re-normalise quaternion coordinates, especially in very long simulations. Since the computational cost of such normalisation is relatively insignificant, it can be done even after every step.

C. Two spheres trapped in translational and rotational harmonic wells

In this section, we explore the time-correlation functions of two harmonically trapped spheres. Their correlated motion arises exclusively due to hydrodynamic interactions. This setting allows us to demonstrate the dynamical consequences of both noise and HI as captured by the integrator, and the crossover to the overdamped limit. The set-up is similar to that in Refs. 25, 33, and 34.

The two spheres with coordinates (r^i, q^i) , $i = 1, 2$, are illustrated in Fig. 3. Unit vectors n^i along the x axis in the body-fixed coordinates of each sphere have space-fixed coordinates $n^i = (n_x^i, n_y^i, n_z^i)^\top = (A_{11}(q^i), A_{12}(q^i), A_{13}(q^i))^\top$, where $A_{kl}(q^i)$ are elements of the rotation matrix (8).

Spheres 1 and 2 are trapped in translational harmonic wells at $(0, 0, 0)^\top$ and $\mathbf{R} = (0, 0, R)^\top$, respectively, as well as in rotational harmonic wells with respect to n_x^i . The potential energy of the system is thus given by (cf. Eq. (4.3) in Ref. 25):

$$U(\mathbf{r}, \mathbf{q}) = \frac{k^t}{2} (|r^1|^2 + |r^2 - \mathbf{R}|^2) - \frac{k^r}{2} [(n_x^1)^2 + (n_x^2)^2]. \quad (38)$$

The translational forces on the two spheres are

$$\begin{aligned} f^1 &= -\nabla_{r^1} U = -k^t r^1, \\ f^2 &= -\nabla_{r^2} U = -k^t (r^2 - \mathbf{R}). \end{aligned} \quad (39)$$

The rotational forces, calculated according to

$$F^i = -\nabla_{q^i} U - (q^{i\top} \nabla_{q^i} U) q^i, \quad (40)$$

$i = 1, 2$, take the form

$$F^i = 4k^r (q_0^{i2} + q_1^{i2} - q_2^{i2} - q_3^{i2}) \begin{pmatrix} q_0^i (q_2^{i2} + q_3^{i2}) \\ q_1^i (q_2^{i2} + q_3^{i2}) \\ -q_2^i (q_0^{i2} + q_1^{i2}) \\ -q_3^i (q_0^{i2} + q_1^{i2}) \end{pmatrix}. \quad (41)$$

Guided by Ref. 33, we compute time-correlation functions (TCFs) among the following variables:

$$\text{transversal modes: } x^1, x^2, \chi_y^1, \chi_y^2, \quad (42)$$

$$\text{longitudinal modes: } z^1, \bar{z}^2, \chi_z^1, \chi_z^2, \quad (43)$$

where $\bar{z}^2 = z^2 - R$ and χ_α^i is the angle of rotation of n^i about the α -axis, so that $\tan \chi_y^i = -n_z^i/n_x^i$ and $\tan \chi_z^i = n_y^i/n_x^i$ (cf. Eqs. (6.3) and (6.4) in Ref. 25).

We use the notation

$$\langle \alpha, \beta \rangle = \frac{\langle \alpha(t + \tau) \beta(t) \rangle}{\sqrt{\langle \alpha^2(t) \rangle \langle \beta^2(t) \rangle}} \quad (44)$$

for the TCF of $\alpha(t)$ and $\beta(t)$.

We computed the following TCFs for pairs of variables formed from the set in (42,43) (taking account of the system symmetry with respect to sphere numbering):

- Auto-correlations: $\langle x^1, x^1 \rangle$, $\langle z^1, z^1 \rangle$, $\langle \chi_y^1, \chi_y^1 \rangle$, $\langle \chi_z^1, \chi_z^1 \rangle$;
- Cross-correlations (between two spheres): $\langle x^1, x^2 \rangle$, $\langle z^1, \bar{z}^2 \rangle$, $\langle \chi_y^1, \chi_y^2 \rangle$, $\langle \chi_z^1, \chi_z^2 \rangle$, $\langle x^1, \chi_y^2 \rangle$;
- Mixed self-correlations: $\langle x^1, \chi_y^1 \rangle$.

All other pairs of variables formed from the set in (43,42) are uncorrelated (see the corresponding discussion in Refs. 25 and 33).

The cross-correlations and mixed self-correlations are the results of the hydrodynamic interaction between the two spheres. Note that mixed self-correlations are zero in the absence of the second sphere³³.

Numerical experiments were carried out on the systems with the following parameters: $m = 1.0$, $I = (0.4, 0.4, 0.4)$, $R = 3.0$ and 3.5 , $k^t = 10.0$, $k^r = 20.0$, and temperatures $k_B T = 0.1$, 0.2 , and 0.5 . We used a relatively small time step of $h = 0.002$ in all simulations.

Figures 4(a) and 5(a) show translational and rotational auto-correlation functions (ACFs). Compared to over-damped dynamics, in which auto-correlations exhibit monotonic exponential decay³³, auto-correlations

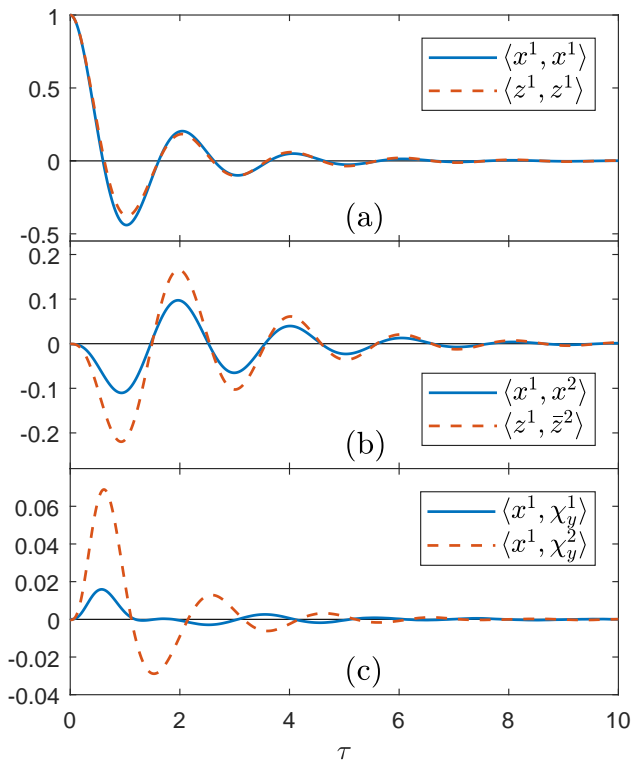


FIG. 4. Translational-translational and translational-rotational TCFs. System parameters: $m = 1.0$, $I = (0.4, 0.4, 0.4)$, $R = 3.0$, $k^t = 10.0$, $k^r = 20.0$, $k_B T = 0.1$. (a) Translational auto-correlation functions. The difference between the ACFs for longitudinal and transversal modes is due to hydrodynamic interactions; (b) Translational cross-correlation functions; (c) Mixed cross-correlation and self-correlation functions. As expected, the self-correlation effect (solid blue line) is weaker than cross-correlation because it is induced by the presence of the second sphere.

in the Langevin dynamics exhibit decaying oscillations which are characteristic of the inertial effects. Crucially, however, we observe the expected cross-correlations and mixed self-correlations with time delay³³. Measurements of the translational and rotational kinetic energies of the spheres confirm thermal equilibration of the system at the correct temperature. We also observe that $\langle (x^i)^2 \rangle = \langle (z^i)^2 \rangle = (k_B T)/k^t$, as expected from the equipartition theorem. The shape of the TCFs shows very weak temperature dependence, while the magnitude of cross-correlations and mixed self-correlations decreases with increasing R .

Because the proposed numerical integrator (27) exactly solves the Ornstein-Uhlenbeck part (19) of the Langevin equations (9)-(10), it can be applied in any hydrodynamic viscosity regime, including high viscosity, where an overdamped dynamical model is typically used. To illustrate this, we have applied our integrator to the system with smaller mass/inertia and energy/temperature, which corresponds to higher viscosity. In Figures 6 and 7 we show the results for the system with parameters which corre-

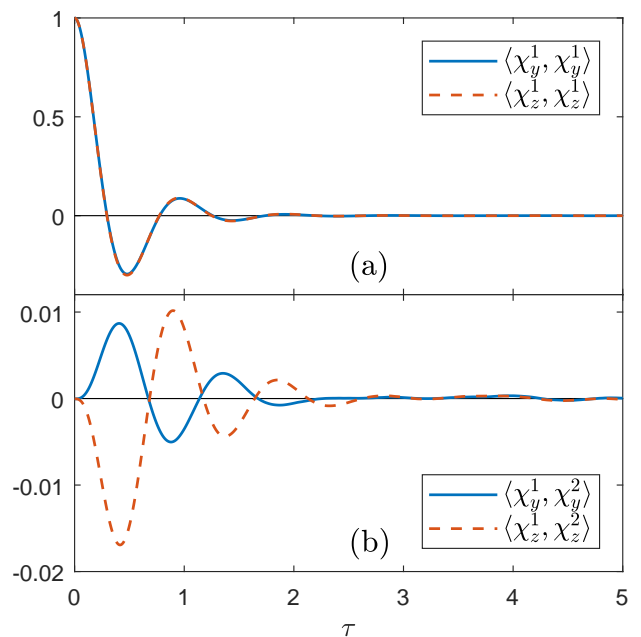


FIG. 5. Rotational TCFs with the same system parameters as in Figure 4. (a) Rotational ACFs. The difference between the ACFs of the rotational longitudinal and transversal modes is very small. (b) Rotational cross-correlation functions.

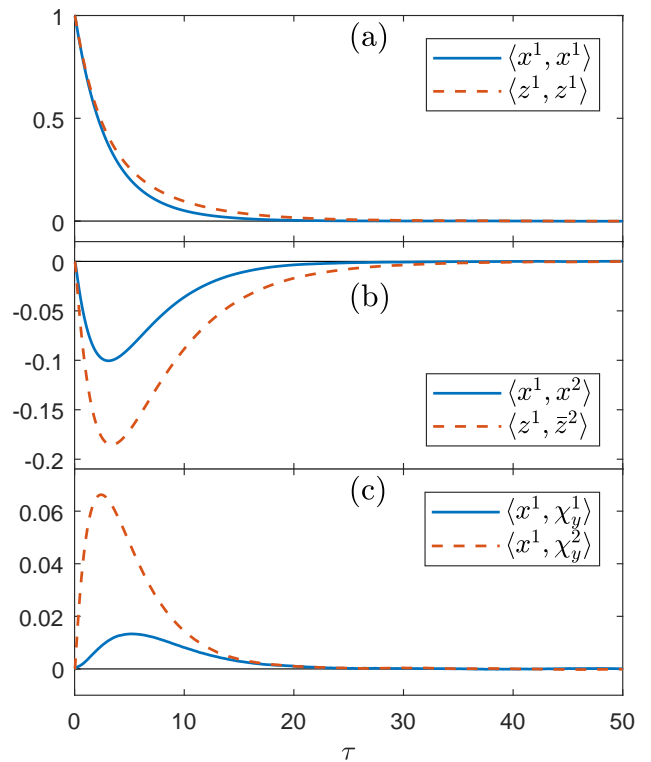


FIG. 6. Same as Figure 4 for the two-sphere system with parameters $m = 0.05$, $I = (0.02, 0.02, 0.02)$, $R = 3.0$, $k^t = 0.5$, $k^r = 1.0$, $k_B T = 0.005$.

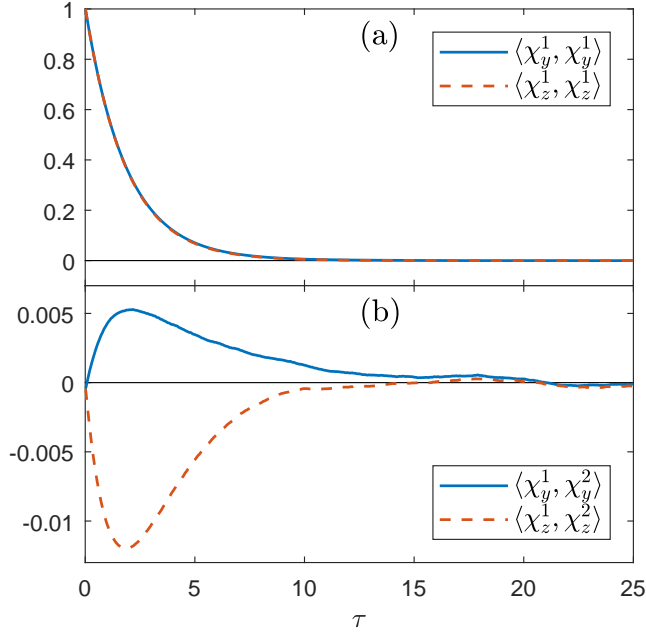


FIG. 7. Same as Figure 5 for the two-sphere system with parameters $m = 0.05$, $I = (0.02, 0.02, 0.02)$, $R = 3.0$, $k^t = 0.5$, $k^r = 1.0$, $k_B T = 0.005$.

spond to 20 times higher viscosity than that shown in Figures 4 and 5. The integration time step is $h = 0.01$. Excellent qualitative agreement of the TCFs with those modelled in Ref. 33 using overdamped dynamics or in experimental measurements^{34–36} is observed. In particular, we note the presence of clearly “anti-correlated” behaviour (see negative TCFs in Figure 6(b)), arising from a resistance to shearing or changing the volume of fluid between the two spheres³³.

D. Circling spheres driven by external force and torque

Here we demonstrate application of our integrator to the system driven by non-conservative forces (see (17)–(18) and Remark IV.2). The set-up is similar to that in Ref. 25. Spheres with coordinates $r^i = (x^i, y^i, z^i)^T$ are placed around a ring of radius R in the x - y plane tethered by a radial harmonic potential and a harmonic potential along the z axis

$$U_{\text{rad}} = \frac{k^t}{2} \sum_{i=1}^N [(\rho^i - R)^2 + (z^i)^2], \quad (45)$$

where N is the number of spheres and $\rho^i = \sqrt{(x^i)^2 + (y^i)^2}$. The spheres interact with one another via a short-range repulsive potential preventing their overlap

$$U_{\text{rep}} = \sum_{i=2}^N \sum_{j=1}^{i-1} A \left[\left(\frac{|r^i - r^j|}{2} \right)^{12} - 1 \right]^{-1}. \quad (46)$$

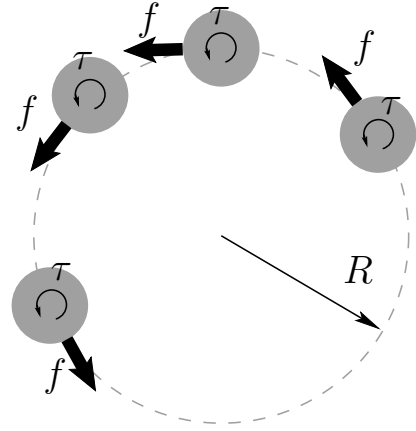


FIG. 8. Spheres circling around a ring of radius R pushed by tangential force f and torques τ .

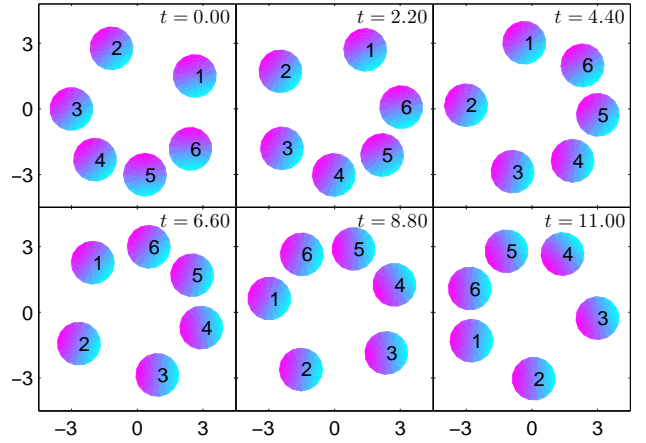


FIG. 9. Illustration of the limit cycle exhibiting drafting effect. $f = 1.0$, $\tau = 0$, $T = 0$. Shading on the spheres indicates their orientation. (Supplementary material: file ring_f1.0tau0T0.mp4).

The repulsive potential is smoothly truncated at the cut-off distance of 2.4 reduced units. In addition, a force with magnitude f is applied to each sphere in the direction tangent to the ring: $(-fy^i/\rho^i, fx^i/\rho^i, 0)^T$ and torque with magnitude τ is applied to spin each sphere in the x - y plane: $(0, 0, \tau)^T$.

In Ref. 25, only noiseless (i.e., $T = 0$) translational dynamics was investigated. Our numerical integrator allows us to investigate the coupling between translational and rotational motion of the spheres, and finite temperature effects. Here we present an example of a system of $N = 6$ spheres on a ring of radius $R = 3.0$. The mass and moments of inertia of each sphere are $m = 1.0$, $I = (0.4, 0.4, 0.4)$. The potential energy constants in Eqs. (45) and (46) are $k^t = 10.0$ and $A = 0.02$, corresponding to relatively strong radial trap and short-range repulsion. We investigate the dependence of the dynamics of this system on parameters f , τ , and T . Since we are

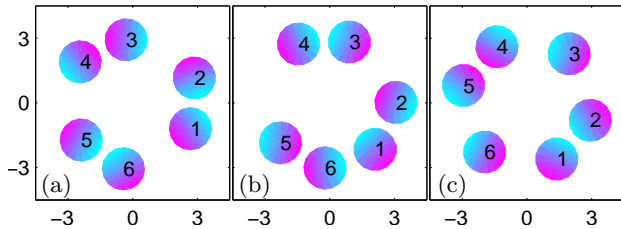


FIG. 10. Illustration of other limiting behaviours of the system with $\tau < 0$. (a) Relative steady state: $f = 1.2$, $\tau = -4.0$ (Supplementary material: file `ring_f1.2tau-4.0T0.mp4`); (b) pair drafting limit cycle: $f = 1.2$, $\tau = -3.0$ (Supplementary material: file `ring_f1.2tau-3.0T0.mp4`); (c) limit cycle with two triplets drafting: $f = 0.4$, $\tau = -4.0$ (Supplementary material: file `ring_f0.4tau-4.0T0.mp4`).

interested in visualizing spheres' trajectories, we rely on the mean-square convergence of the method (27) appropriately modified for the system with non-conservative forces (see Remark IV.2).

For $f > 0$, $\tau = 0$, and $T = 0$, the spheres move around the ring anticlockwise in a limit cycle exhibiting a drafting effect²⁵, where a cluster of five spheres moves faster and catches up the sixth sphere, while the trailing sphere in the cluster gets dropped, as shown in Figure 9 (see also the corresponding video in [supplementary material](#)). Due to the hydrodynamic coupling between translational and rotational degrees of freedom, the spheres also spin anticlockwise in the x - y plane (as seen by the shading of the spheres). The sphere velocities around the ring and the spin angular velocities increase with increasing f . Note that the induced rotation of the spheres in turn influences the translational velocity around the ring, emphasising the importance of considering rotational motion even in the absence of the torque ($\tau = 0$).

The drafting limit cycle persists for $\tau > 0$, with the spheres spinning faster and moving faster anticlockwise around the ring. However, when $\tau < 0$, the spheres are pushed to spin clockwise, causing disruption of the limit cycle through hydrodynamic interactions and the emergence of other asymptotic behaviours, shown in Figure 10 and in [supplementary material](#). The most common is the relative steady state solution (i.e. relative with respect to the orbital rotation symmetry), shown in Figure 10(a), where spheres move in pairs around the ring at fixed distances, constant spin angular velocities (clockwise), and constant orbiting velocity.

Other types of limit cycles are observed in the (f, τ) parameter plane, usually on the boundaries between the drafting limit cycle in Figure 9 and the steady state solution in Figure 10(a). For $f = 0$ and $\tau \neq 0$, a different type of drafting limit cycle is observed, where the spinning of the spheres induces, through the hydrodynamic coupling, orbital motion around the ring (see [supplementary material](#): file `[ring_f0tau-5.0aT0.mp4]`). At relatively large f and somewhat weaker negative τ compared to the steady state solution, we observe a drafting limit cycle

shown in Figure 10(b), where a pair of trailing spheres detaches from the back of the faster moving cluster of four spheres and then is recaptured while another pair of spheres is dropped at the back. For weaker f and relatively strong τ , yet another type of a drafting limit cycle is observed where spheres move in triplets as shown Figure 10(c): spheres are orbiting clockwise with spheres 3 and 6 getting caught by faster moving pairs 4,5 and 2,1, respectively, followed by spheres 5 and 2 getting dropped at the back of the moving triplets.

With $T > 0$, noise is introduced into the system. Different types of limit cycles exhibit different degrees of sensitivity to noise. For $k_B T \lesssim 0.0001$, all limit cycles discussed above can still be observed, while for $k_B T \gtrsim 0.001$ we mostly observe the limit cycle shown in Figure 9 and the steady state shown in Figure 10(a) (Supplementary material: files `ring_f1.0tau0T0.01.mp4` and `ring_f1.2tau-4.0T0.01.mp4`). Close to the boundary between the two solutions in the (f, τ) parameter plane, we also observe the system switching between the two solutions at random time intervals. Such behaviour can be characterised as noise-induced intermittency³⁷.

VI. CONCLUSIONS

We have proposed and tested a quaternion-based geometric integrator for Langevin SDEs that incorporates cooperative hydrodynamic interactions between rigid bodies. The integrator takes a user-defined approximation to the multi-particle friction tensor as an input, does not assume the overdamped limit, and is of second order in the weak sense. Further, the integrator naturally conserves quaternion length and is symplectic in the noise-free, friction-free limit. To our knowledge, this is the first quaternion-based integrator incorporating cooperative hydrodynamics that has been implemented and tested.

Langevin dynamics with hydrodynamic interactions (so-called Stokesian dynamics) is widely used to understand a range of systems, including the rheology of colloidal suspensions and cellular transport^{7,9,10}. Our method will facilitate the incorporation of rotational motion into these descriptions, which is important for modelling, e.g. patchy colloids³⁸⁻⁴¹ and globular proteins^{9,10}.

Historically, Stokesian integrators have assumed an over-damped (“Brownian”) limit in which the inertia of the simulated particles is neglected^{1,13-15,18}. By contrast, our algorithm explicitly retains the generalised momenta; the over-damped limit can be approached simply by setting friction coefficients to large values. This setup allows the construction of a Verlet-like integrator with second-order weak accuracy in the time-step. We expect that this approach will be particularly useful in two contexts. Firstly, it will allow the study of systems that are not over-damped; such systems can show substantially different behaviour from their over-damped counterparts⁴².

Alternatively, in systems with stiff interactions, it is

important to accurately integrate the potential forces that contribute to the equations of motion by using small time steps. As was observed, for example, in Ref. 17 and 19, the use of Brownian dynamics is often hindered by inefficiency of numerical integrators which, under the requirement of a single evaluation of the forces and friction matrix per step of an algorithm, are only of weak first-order accuracy in comparison with second-order weak numerical schemes available for Langevin systems. Consequently, the combination of Langevin equations and a second-order geometric integrator is usually more computationally efficient than the combination of Brownian dynamics and a first-order scheme. We therefore expect that the numerical method proposed in this paper will be a powerful tool for studying the over-damped limit, just as similar second-order integrators (without HI) have been successfully used to simulate coarse-grained models with stiff potential functions^{43–46}.

Our approach is particularly suited to studying small systems using accurate hydrodynamic models; depending on the accuracy required, larger systems may be better treated by methods such as Lattice Boltzmann⁴⁷, Dissipative Particle Dynamics⁴⁸ or Multiparticle Collision Dynamics⁴⁹, which use a simplified but explicit representation of the solvent. In particular, we note that models of externally-driven colloids or self-propelled swimmers rely on the hydrodynamic interaction between only a few bodies to produce interesting phenomena^{11,24,25}. Some work has been done to understand the potential importance of noise for swimmers^{24,50}; our algorithm allows the incorporation of both rotational motion and inertia into this perspective, as we have shown in the particular case of spheres driven round a ring.

A second obvious use of our approach in the context of small systems is in studying self-assembly. Recently, several authors have highlighted the important role of diffusion in determining the self-assembly pathways of finite-sized structures in the absence of cooperative hydrodynamics^{41,51}. Our integrator would enable this analysis to be extended to self-assembling systems with hydrodynamic interactions.

SUPPLEMENTARY MATERIAL

See supplementary material for videos of the dynamical behaviour of spheres moving on a ring under the influence of orbital force and a spinning torque, as discussed in Section V D.

ACKNOWLEDGMENT

This work was partially supported by the Computer Simulation of Condensed Phases (CCP5) Collaboration Grant, which is part of the EPSRC grant EP/J010480/1. T.E.O. is supported by a Royal Society University Research Fellowship, and also acknowledges fellowships

from University College, Oxford and Imperial College London. R.L.D. acknowledges a study leave granted by the University of Leicester. This research used the ALICE High Performance Computing Facility at the University of Leicester.

Appendix A: Evaluation of covariance integral and matrix σ

Let us rewrite $\tilde{\xi}(\mathbf{r}, \mathbf{q})$ as

$$\tilde{\xi}(\mathbf{r}, \mathbf{q}) = G_1(\mathbf{q})\xi(\mathbf{r}, \mathbf{q})G_2(\mathbf{q}), \quad (\text{A1})$$

where the $7n$ -by- $6n$ matrix G_1 and the $6n$ -by- $7n$ matrix G_2 have the following block structure

$$G_1(\mathbf{q}) = \begin{bmatrix} \mathbf{1}_{3n} & \mathbf{0} \\ \mathbf{0} & G_{11}(\mathbf{q}) \end{bmatrix}, \quad G_2(\mathbf{q}) = \begin{bmatrix} G_{21} & \mathbf{0} \\ \mathbf{0} & G_{22}(\mathbf{q}) \end{bmatrix}. \quad (\text{A2})$$

Here $\mathbf{0}$ are zero matrices of the corresponding dimensions, $\mathbf{1}_{3n}$ is the $3n$ -dimensional identity matrix, G_{11} is the $4n$ -by- $3n$ block-diagonal matrix with diagonal 4-by-3 blocks

$$G_{11}^{(i,i)}(\mathbf{q}) = 2\check{S}(q^i), \quad i = 1, \dots, n, \quad (\text{A3})$$

G_{21} is the $3n$ -by- $3n$ diagonal matrix with the 3-by-3 diagonal blocks

$$G_{21}^{(j,j)} = \frac{1}{m^j} \mathbf{1}_3, \quad j = 1, \dots, n, \quad (\text{A4})$$

and G_{22} is the $3n$ -by- $4n$ block-diagonal matrix with the diagonal 3-by-4 blocks

$$G_{22}^{(j,j)} = \frac{1}{2} A^\top(q^j) \hat{D}^j \hat{S}^\top(q^j), \quad j = 1, \dots, n. \quad (\text{A5})$$

We can also rewrite $\tilde{b}(\mathbf{r}, \mathbf{q})$ as

$$\tilde{b}(\mathbf{r}, \mathbf{q}) = G_1(\mathbf{q})b(\mathbf{r}, \mathbf{q}) \quad (\text{A6})$$

and thus, using Eq. (15),

$$\tilde{b}(\mathbf{r}, \mathbf{q})\tilde{b}^\top(\mathbf{r}, \mathbf{q}) = \frac{2}{\beta} G_1(\mathbf{q})\xi(\mathbf{r}, \mathbf{q})G_1^\top(\mathbf{q}). \quad (\text{A7})$$

In addition we define the $6n$ -by- $6n$ matrix

$$K := G_2G_1 = \begin{bmatrix} G_{21} & \mathbf{0} \\ \mathbf{0} & K_2(\mathbf{q}) \end{bmatrix}, \quad (\text{A8})$$

where $K_2 := G_{22}(\mathbf{q})G_{11}(\mathbf{q})$. The 3-by-3 blocks on the main diagonal of K_2 have the form

$$A^\top(q^j) \hat{D}^j \hat{S}^\top(q^j) \check{S}(q^j) = A^\top(q^j) \hat{D}^j A(q^j). \quad (\text{A9})$$

Therefore, both K_2 and K are symmetric:

$$K = K^\top = G_1^\top G_1^\top. \quad (\text{A10})$$

Using the definition of the matrix exponent and properties of the above defined matrices, we have

$$e^{-\tilde{\xi}(t-s)}G_1\xi = G_1\xi e^{-K\xi(t-s)}$$

as well as

$$G_1^\top e^{-\tilde{\xi}^\top(t-s)} = e^{-K\xi(t-s)}G_1^\top.$$

Thus, the covariance integral in Eq. (24) can be evaluated as follows

$$\begin{aligned} C(t; \mathbf{r}, \mathbf{q}) &= \int_0^t e^{-\tilde{\xi}(\mathbf{r}, \mathbf{q})(t-s)} \tilde{b}(\mathbf{r}, \mathbf{q}) \tilde{b}(\mathbf{r}, \mathbf{q})^\top e^{-\tilde{\xi}(\mathbf{r}, \mathbf{q})^\top(t-s)} ds \\ &= \frac{2}{\beta} G_1(\mathbf{q}) \xi(\mathbf{r}, \mathbf{q}) \left[\int_0^t e^{-2K(\mathbf{q})\xi(\mathbf{r}, \mathbf{q})(t-s)} ds \right] G_1^\top(\mathbf{q}) \\ &= \frac{1}{\beta} G_1(\mathbf{q}) \xi(\mathbf{r}, \mathbf{q}) [K(\mathbf{q})\xi(\mathbf{r}, \mathbf{q})]^{-1} \\ &\quad \times \left[\mathbf{1}_{6n} - e^{-2K(\mathbf{q})\xi(\mathbf{r}, \mathbf{q})t} \right] G_1^\top(\mathbf{q}) \\ &= \frac{1}{\beta} G_1(\mathbf{q}) K^{-1}(\mathbf{q}) \left[\mathbf{1}_{6n} - e^{-2K(\mathbf{q})\xi(\mathbf{r}, \mathbf{q})t} \right] G_1^\top(\mathbf{q}). \end{aligned}$$

Note that

$$K^{-1}(\mathbf{q}) = \begin{bmatrix} G_{21}^{-1} & \mathbf{0} \\ \mathbf{0} & K_2^{-1}(\mathbf{q}) \end{bmatrix}, \quad (\text{A11})$$

which is easy to compute analytically since G_{21} is diagonal and $K_2(\mathbf{q})$ is block diagonal with blocks on the diagonal being $A^\top(q^j)\hat{D}^j A(q^j)$ and

$$\left[A^\top(q^j)\hat{D}^j A(q^j) \right]^{-1} = A^\top(q^j) \left[\hat{D}^j \right]^{-1} A(q^j). \quad (\text{A12})$$

We can now write the matrix $\sigma(t; \mathbf{r}, \mathbf{q})$ in Eq. (25) in the form

$$\sigma(t; \mathbf{r}, \mathbf{q}) = \frac{1}{\sqrt{\beta}} G_1(\mathbf{q}) \tilde{\sigma}(t; \mathbf{r}, \mathbf{q}), \quad (\text{A13})$$

where the $6n$ -by- $6n$ matrix $\tilde{\sigma}(t; \mathbf{r}, \mathbf{q})$ satisfies

$$\tilde{\sigma}(t; \mathbf{r}, \mathbf{q}) \tilde{\sigma}^\top(t; \mathbf{r}, \mathbf{q}) = K^{-1}(\mathbf{q}) \left[\mathbf{1}_{6n} - e^{-2K(\mathbf{q})\xi(\mathbf{r}, \mathbf{q})t} \right] \quad (\text{A14})$$

which can be computed by Cholesky factorization.

We also note that the matrix exponent $e^{-\tilde{\xi}(\mathbf{r}, \mathbf{q})t}$ from (26), which is used in the method (27), can be expressed as

$$\begin{aligned} e^{-\tilde{\xi}(\mathbf{r}, \mathbf{q})t} &= G_1(\mathbf{q}) \left[e^{-K(\mathbf{q})\xi(\mathbf{r}, \mathbf{q})t} \right]^\top G_1^\top(\mathbf{q}) \begin{bmatrix} \mathbf{1}_{3n} & \mathbf{0} \\ \mathbf{0} & \mathbf{1}_{4n}/4 \end{bmatrix} \\ &\quad + \begin{bmatrix} \mathbf{0} & \mathbf{0} \\ \mathbf{0} & \mathbf{q}\mathbf{q}^\top \end{bmatrix}, \end{aligned}$$

where $\mathbf{q}\mathbf{q}^\top$ means the block diagonal matrix with 4×4 blocks being $(q^j)(q^j)^\top$. That is, per step of (27) we only need to compute one matrix exponent, $e^{-K(\mathbf{q})\xi(\mathbf{r}, \mathbf{q})t}$. However, in Appendix B we present, for better clarity, the implementation with two matrix exponents.

Appendix B: Implementation details of the numerical integrator

The numerical integrator (27) was implemented in Fortran 90, using the HYDROLIB package³⁰ to compute the friction matrix $\xi(\mathbf{r})$ and EXPOKIT⁵² subroutine `dgpadm` to evaluate matrix exponents. LAPACK subroutine `dpotrf` was used to compute Cholesky factorisation. Below we provide the implementation details. The Ziggurat random number generator^{53,54} was used for generating the Gaussian distribution.

HYDROLIB defines the number of particles variable `_NP_` and global arrays for particle center-of-mass coordinates `c(0:2,1:_NP_)`, linear and angular velocities `v(1:6*_NP_)`, forces and torques `f(1:6*_NP_)`, and the friction matrix `fr(1:6*_NP_,1:6*_NP_)`. Specifically, `c(0:2,i)` contains components of r^i , `v(6*i-5:6*i-3)` contains p^i/m^i , and `f(6*i-5:6*i-3)` contains f^i . The angular velocity and torque components in `v` and `f` are not used. Instead, we define global variables `qq(0:3,1:_NP_)`, `qp(0:3,1:_NP_)`, and `qf(0:3,1:_NP_)` containing q^i , π^i , and F^i , respectively, $i = 1, \dots, n$. Particles masses m^i and principal moments of inertia $I^i = (I_1^i, I_2^i, I_3^i)^\top$, $i = 1, \dots, n$, are stored in arrays `mass(1:_NP_)` and `inert(1:3,1:_NP_)`, respectively. The structure of array `fr` is described in the HYDROLIB guide.

SUBROUTINE OneStep

```
! one step of numerical integrator (27)
hh = h/2
do i = 1, _NP_
  i1 = 6*i-5; i2 = i1+2
  v(i1:i2) = v(i1:i2) + hh*f(i1:i2)/mass(i)
  qp(:,i) = qp(:,i) + hh*qf(:,i)
  c(:,i) = c(:,i) + hh*v(i1:i2)
end do
CALL FreeRotorMinus(hh)
CALL OUStep(h)
do i = 1, _NP_
  i1 = 6*i-5; i2 = i1+2
  c(:,i) = c(:,i) + hh*v(i1:i2)
end do
CALL FreeRotorPlus(hh)
CALL ComputeForces
do i = 1, _NP_
  i1 = 6*i-5; i2 = i1+2
  v(i1:i2) = v(i1:i2) + hh*f(i1:i2)/mass(i)
  qp(:,i) = qp(:,i) + hh*qf(:,i)
end do
END SUBROUTINE OneStep
```

SUBROUTINE FreeRotorMinus(dt)

```
! compute map  $\Psi_t^-$  in Eq. (29)
do i = 1, _NP_
  CALL Rotate(3, dt, i)
  CALL Rotate(2, dt, i)
  CALL Rotate(1, dt, i)
end do
```

```

end do
END SUBROUTINE FreeRotorMinus

```

```

SUBROUTINE FreeRotorPlus(dt)
! compute map  $\Psi_t^+$  in Eq. (29)
do i = 1, _NP_
  CALL Rotate(1, dt, i)
  CALL Rotate(2, dt, i)
  CALL Rotate(3, dt, i)
end do
END SUBROUTINE FreeRotorPlus

```

```

SUBROUTINE Rotate(1, dt, i)
! compute map in Eq. (28)
sq = Slq(1, qq(:,i))
sp = Slq(1, qp(:,i))
zdt = dt*dot_product(qp(:,i),sq)/inert(1,i)/4
qq(:,i) = cos(zdt)*qq(:,i) + sin(zdt)*sq
qp(:,i) = cos(zdt)*qp(:,i) + sin(zdt)*sp
END SUBROUTINE Rotate

```

```

FUNCTION Slq(1, q)
if (1 == 1) then
  Slq(0:3) = [-q(1), q(0), q(3), -q(2)]
else if (1 == 2) then
  Slq(0:3) = [-q(2), -q(3), q(0), q(1)]
else ! 1 == 3
  Slq(0:3) = [-q(3), q(2), -q(1), q(0)]
end if
END FUNCTION Slq

```

```

SUBROUTINE OUStep(h)
! compute Ornstein-Unlenbeck step ! HYDROLIB
call: compute  $\xi(r)$ , output in fr
  CALL Eval
! compute  $\xi(r, q)$  in Eq. (20), output in etxi
do j = 1, _NP_
! compute  $A^\top(q^j)\hat{D}^j\hat{S}^\top(q^j)$ , output in ads
  ads = transpose(HatSq(j))
  ads(1,:) = ads(1,+)/inert(1,j)
  ads(2,:) = ads(2,+)/inert(2,j)
  ads(3,:) = ads(3,+)/inert(3,j)
  ads = matmul(transpose(RotMat(j),ads)
  kj = 6*j-5; mj = 7*j-6
  do i = 1, _NP_
    ki = 6*i-5; mi = 7*i-6
    etxi(mi:mi+2,mj:mj+2) =
fr(ki:ki+2,kj:kj+2)/mass(j) ! tt
    etxi(mi:mi+2,mj+3:mj+6) =
matmul(fr(ki:ki+2,kj+3:kj+5),ads)/2 ! tr
    etxi(mi+3:mi+6,mj:mj+2) =
matmul(CheckSq(i),
fr(ki+3:ki+5,kj:kj+2))*2/mass(j) ! rt
    etxi(mi+3:mi+6,mj+3:mj+6) =
matmul(CheckSq(i),
matmul(fr(ki+3:ki+5,kj+3:kj+5),ads)) ! rr
  end do
end do

```

```

! compute  $e^{-h\tilde{\xi}(r,q)}$ , output in etxi
  CALL ExpMat(-h, 7*_NP_, etxi, etxi)
! compute  $K\xi$ , output in cc
  do i = 1, _NP_
! compute  $A^\top(q^i)\hat{D}^iA(q^i)$ , output in ada
    aa = RotMat(i) !  $A(q^i)$ 
    do l = 1, 3
      ada(l,:) = aa(l,+)/inert(1,i)
    end do
    ada = matmul(transpose(aa),ada)
    ki = 6*i-5
    do j = 1, _NP_
      kj = 6*j-5
      cc(ki:ki+2,kj:kj+5) =
fr(ki:ki+2,kj:kj+5)/mass(i) ! tt, tr
      cc(ki+3:ki+5,kj:kj+2) = matmul(ada,
fr(ki+3:ki+5,kj:kj+2)) ! rt
      cc(ki+3:ki+5,kj+3:kj+5) = matmul(ada,
fr(ki+3:ki+5,kj+3:kj+5)) ! rr
    end do
  end do
! compute  $e^{-2hK\xi}$ , output in cc
  CALL ExpMat(-2*h, 6*_NP_, cc, cc)
! compute  $-K^{-1}[e^{-2hK\xi} - \mathbf{1}_{6n}]$ , output in cc
  do ki = 1, 6*_NP_
    cc(ki,ki) = cc(ki,ki) - 1
  end do
  do i = 1, _NP_
! compute  $-A^\top(q^i)[\hat{D}^i]^{-1}A(q^i)$ , output in ada
    aa = RotMat(i) !  $A(q^i)$ 
    do l = 1, 3
      ada(l,:) = -inert(1,i)*aa(l,:)
    end do
    ada = matmul(transpose(aa), ada)
    ki = 6*i-5
    do j = 1, _NP_
      kj = 6*j-5
      cc(ki:ki+2,kj:kj+5) =
-mass(i)*cc(it:tr+2,jt:jr+2) ! tt, tr
      cc(ki+3:ki+5,kj:kj+2) =
matmul(ada,cc(ki+3:ki+5,kj:kj+2)) ! rt
      cc(ki+3:ki+5,kj+3:kj+5) =
matmul(ada,cc(ki+3:ki+5,kj+3:kj+5)) ! rr
    end do
  end do
! compute  $\tilde{\sigma}$  by Cholesky factorization, output
in cc
  CALL dpotrf('L', 6*_NP_, cc, 6*_NP_, info)
  do i = 1, 6*_NP_-1
    cc(i,i+1:6*_NP_) = 0
  end do
! compute  $G_1\tilde{\sigma}$ , output in sigma
  sigma = 0
  do i = 1, _NP_
    cs = 2*CheckSq(i) !  $2\check{S}(q^i)$ 
    ki = 6*i-5; mi = 7*i-6
    do j = 1, i

```

```

    kj = 6*(j-1)+1
    sigma(mi:mi+2,kj:kj+5) =
cc(ki:ki+2,kj:kj+5) ! tt, tr
    sigma(mi+3:mi+6,kj:kj+2) =
matmul(cs,cc(ki+3:ki+5,kj:kj+2)) ! rt
    sigma(mi+3:mi+6,kj+3:kj+5) =
matmul(cs,cc(ki+3:ki+5,kj+3:kj+5)) ! rr
    end do
end do
! define  $Y = (\mathbf{r}^T, \mathbf{q}^T)^T$ , output in yy
do i = 1, _NP_
    ki = 6*i-5; mi = 7*i-6
    yy(mi:mi+2) = mass(i)*v(ki:ki+2)
    yy(mi+3:mi+6) = qp(:,i)
end do
! compute  $e^{-h\tilde{\xi}Y}$ , output in yy
yy = matmul(etxi, yy)
! generate  $\chi$  with i.i.d.  $\mathcal{N}(0,1)$  components
CALL RandNiid(6*_NP_, chi)
! add  $\sigma(h; \mathbf{r}, \mathbf{q})\chi$ 
yy = yy + matmul(sigma, sqrt(tempr)*chi)
! copy from yy back to v and qp
do i = 1, _NP_
    ki = 6*i-5; mi = 7*i-6
    v(ki:ki+2) = Y(mi:mi+2)/mass(i)
    qp(:,i) = Y(mi+3:mi+6)
end do
END SUBROUTINE OUStep

SUBROUTINE ExpMat(t, n, hh, ethh)
! compute  $\exp(t*hh(1:n,1:n))$ , output in ethh
integer, parameter :: ideg = 6
real :: wsp(4*n*n+ideg+1), ipiv(n)
lwsp = 4*n*n+ideg+1
! EXPOKIT subroutine
CALL dgpadm(ideg,n,t,hh,n,wsp,lwsp,ipiv,iexph,
ns,iflag)
ethh = reshape(wsp(iexph:iexph+n*n-1), [n, n])
END SUBROUTINE ExpMat

SUBROUTINE RandNiid(n, rnd)
do i = 1, n
! call function from ziggurat.f9054
    rnd(i) = r4_nor(seed, kn, fn, wn)
end do
END SUBROUTINE RandNiid

FUNCTION RotMat(i)
k = 0
do l = 0, 3
do m = 1, 3
k = k + 1
p(k) = 2*qq(l,i)*qq(m,i)
end do
end do
RotMat(1,1:3) = [p(1)+p(5)-1, p(6)+p(4),
p(7)-p(3)]
RotMat(2,1:3) = [p(6)+p(4), p(1)+p(8)-1,

```

```

p(9)+p(2)]
RotMat(3,1:3) = [p(7)+p(3), p(9)-p(2),
p(1)+p(10)-1]
END FUNCTION RotMat

FUNCTION HatSq(i)
HatSq(:,1) = [-qq(1,i), qq(0,i), qq(3,i),
-qq(2,i)]
HatSq(:,2) = [-qq(2,i), -qq(3,i), qq(0,i),
qq(1,i)]
HatSq(:,3) = [-qq(3,i), qq(2,i), -qq(1,i),
qq(0,i)]
END FUNCTION HatSq(i)

FUNCTION CheckSq(i)
S(:,1) = [-qq(1,i), qq(0,i), -qq(3,i),
qq(2,i)]
S(:,2) = [-qq(2,i), qq(3,i), qq(0,i),
-qq(1,i)]
S(:,3) = [-qq(3,i), -qq(2,i), qq(1,i),
qq(0,i)]
END FUNCTION CheckSq(i)

```

- ¹I. Snook, *The Langevin and Generalised Langevin Approach to the Dynamics of Atomic, Polymeric and Colloidal Systems* (Elsevier, 2006).
- ²T. E. Ouldridge, arXiv:1702.00360 (2017).
- ³D. Frenkel and B. Smit, *Understanding Molecular Simulation*, 2nd ed. (Academic Press, New York, 2002).
- ⁴G. N. Milstein and M. V. Tretyakov, *Physica D* **229**, 81 (2007).
- ⁵N. G. Van Kampen, *Stochastic processes in physics and chemistry* (Elsevier, Amsterdam, 2007).
- ⁶B. H. Zimm, *J. Chem. Phys.* **24**, 269 (1956).
- ⁷J. D. Park, J. S. Myung, and K. H. Ahn, *Korean. J. Chem. Eng.* **33**, 3069 (2016).
- ⁸G. K. Batchelor, *J. Fluid Mech.* **52**, 245 (1971).
- ⁹M. Długosz and J. Trylska, *BMC Biophysics* **4**, 3 (2011).
- ¹⁰J. Skolnick, *J. Chem. Phys.* **145**, 100901 (2016).
- ¹¹A. Najafi and R. Golestanian, *Phys. Rev. E* **69**, 062901 (2004).
- ¹²C. M. Polley, G. P. Alexander, and J. M. Yeomans, *Phys. Rev. Lett.* **99**, 228103 (2007).
- ¹³D. Ermak and J. McCammon, *J. Chem. Phys.* **69**, 1352 (1978).
- ¹⁴E. Dickinson, S. A. Allison, and J. A. McCammon, *J. Chem. Soc. Faraday Trans.* **81**, 591 (1985).
- ¹⁵J. F. Brady and G. Bossis, *Ann. Rev. Fluid Mech.* **20**, 111 (1988).
- ¹⁶D. J. Evans, *Mol. Phys.* **34**, 317 (1977).
- ¹⁷R. L. Davidchack, R. Handel, and M. V. Tretyakov, *J. Chem. Phys.* **130**, 234101 (2009).
- ¹⁸I. M. Ilie, W. J. Briels, and W. K. den Otter, *J. Chem. Phys.* **142**, 114103 (2015).
- ¹⁹R. L. Davidchack, T. E. Ouldridge, and M. V. Tretyakov, *J. Chem. Phys.* **142**, 144114 (2015).
- ²⁰T. F. Miller III, M. Eleftheriou, P. Pattnaik, A. Ndirango, D. Newns, and G. J. Martyna, *J. Chem. Phys.* **116**, 8649 (2002).
- ²¹R. Kutteh, *J. Chem. Phys.* **132**, 174107 (2010).
- ²²R. Z. Hasminskii, *Stochastic Stability of Differential Equations* (Sijthoff & Noordhoff, 1980).
- ²³C. Soize, *The Fokker-Planck Equation for Stochastic Dynamical Systems and Its Explicit Steady State Solutions* (World Scientific, Singapore, 1994).
- ²⁴J. Dunkel and I. M. Zaid, *Phys. Rev. E* **80**, 021903 (2009).
- ²⁵M. Reichert, *Hydrodynamic Interactions in Colloidal and Biological Systems*, Ph.D. thesis, University of Constance, Germany (2006).

- ²⁶R. Joubad, G. A. Pavliotis, and G. Stoltz, *J. Stat. Phys.* **158**, 1 (2015).
- ²⁷G. N. Milstein and M. V. Tretyakov, *Stochastic Numerics for Mathematical Physics* (Springer, Berlin, 2004).
- ²⁸G. N. Milstein and M. V. Tretyakov, *IMA J. Numer. Anal.* **23**, 593 (2003).
- ²⁹G. N. Milstein and M. V. Tretyakov, *SIAM J. Sci. Comput.* **18**, 1067 (1997).
- ³⁰K. Hinsen, *Comput. Phys. Commun.* **88**, 327 (1995), the Fortran source code is available at <http://dirac.cnrs-orleans.fr/HYDROLIB>.
- ³¹B. Cichocki, B. U. Felderhof, K. Hinsen, E. Wajnryb, and J. Bławdziewicz, *J. Chem. Phys.* **100**, 3780 (1994).
- ³²J. Happel and H. Brenner, *Low Reynolds number hydrodynamics: with special applications to particulate media*, Mechanics of Fluids and Transport Processes (Springer, Netherlands, 1983).
- ³³M. Reichert and H. Stark, *Phys. Rev. E* **69**, 031407 (2004).
- ³⁴S. Martin, M. Reichert, H. Stark, and T. Gisler, *Phys. Rev. Lett.* **97**, 248301 (2006).
- ³⁵J.-C. Meiners and S. R. Quake, *Phys. Rev. Lett.* **82**, 2211 (1999).
- ³⁶P. Bartlett, S. I. Henderson, and S. J. Mitchell, *Phil. Trans. R. Soc. London A* **359**, 883 (2001).
- ³⁷J. P. Eckmann, L. Thomas, and P. Wittwer, *J. Phys. A: Math. Gen.* **14**, 3153 (1981).
- ³⁸S. C. Glotzer and M. J. Solomon, *Nat. Mater.* **6**, 557 (2007).
- ³⁹A. B. Pawar and I. Kretzschmar, *Macromol. Rapid Commun.* **31**, 150 (2010).
- ⁴⁰Q. Chen, S. C. Bae, and S. Granick, *Nature* **469**, 381 (2011).
- ⁴¹A. C. Newton, J. Groenewold, W. K. Kegel, and P. G. Bolhuis, *Proc. Nat. Acad. Sci. USA* **112**, 15308 (2015), <http://www.pnas.org/content/112/50/15308.full.pdf>.
- ⁴²B. Ai and F. Li, *Soft Matter* **13**, 2536 (2017).
- ⁴³F. Takagi, N. Koga, and S. Takada, *Proc. Nat. Acad. Sci. USA* **100**, 11367 (2003).
- ⁴⁴T. E. Ouldridge, R. L. Hoare, A. A. Louis, J. P. K. Doye, J. Bath, and A. J. Turberfield, *ACS Nano* **7**, 2479 (2013).
- ⁴⁵R. R. F. Machinek, T. E. Ouldridge, N. E. C. Haley, J. Bath, and A. J. Turberfield, *Nat. Commun.* **5**, 5324 (2014).
- ⁴⁶D. Hinckley, J. P. Lequieu, and J. J. de Pablo, *J. Chem. Phys.* **141**, 035102 (2014).
- ⁴⁷A. J. C. Ladd, *Phys. Rev. Lett.* **70**, 1339 (1993).
- ⁴⁸R. D. Groot and P. B. Warren, *J. Chem. Phys.* **107**, 4423 (1997).
- ⁴⁹A. Malavanets and R. Kapral, *J. Chem. Phys.* **110**, 8605 (1999).
- ⁵⁰E. Lauga, *Phys. Rev. Lett.* **106**, 178101 (2011).
- ⁵¹A. Vijaykumar, P. G. Bolhuis, and R. ten Wolde, *Faraday Discuss.* **195**, 421 (2016).
- ⁵²R. B. Sidje, *ACM Trans. Math. Softw.* **24**, 130 (1998).
- ⁵³G. Marsaglia and W. W. Tsang, *J. Stat. Softw.* **5**, 1 (2000).
- ⁵⁴“Ziggurat Fortran 90 library by John Burkardt,” http://people.sc.fsu.edu/~jburkardt/f_src/ziggurat/ziggurat.html.